UNIVERSIDAD DE INVESTIGACIÓN DE TECNOLOGÍA EXPERIMENTAL YACHAY

Escuela de Ciencias Químicas e Ingeniería

Design of a Pilot Scale Sand Filter to Evaluate the Color Removal Capacity of Iron-Titaniferous Sands of Ecuador in Textile Effluents

Trabajo de integración curricular presentado como requisito para la obtención del título de Petroquímico

Autor:

Cobo Espinosa Joseph Andrés

Tutor:

Ph.D Viloria Vera Darío Alfredo

Co-tutor:

Ph.D Ricaurte Fernández Marvin José

Urcuquí, Septiembre del 2020

SECRETARÍA GENERAL
(Vicerrectorado Académico/Cancillería)
ESCUELA DE CIENCIAS QUÍMICAS E INGENIERÍA
CARRERA DE PETROQUÍMICA
ACTA DE DEFENSA No. UITEY-CHE-2020-00047-AD

A los 25 días del mes de septiembre de 2020, a las 16:30 horas, de manera virtual mediante videoconferencia, y ante el Tribunal Calificador, integrado por los docentes:

Presidente Tribunal de Defensa	Dr. CAETANO SOUSA MANUEL , Ph.D.
Miembro No Tutor	Dr. SOMMER MARQUEZ, ALICIA ESTELA , Ph.D.
Tutor	Dr. VILORIA VERA, DARIO ALFREDO , Ph.D.

El(la) señor(ita) estudiante **COBO ESPINOSA, JOSEPH ANDRES**, con cédula de identidad No. **1804127296**, de la **ESCUELA DE CIENCIAS QUÍMICAS E INGENIERÍA**, de la Carrera de **PETROQUÍMICA**, aprobada por el Consejo de Educación Superior (CES), mediante Resolución **RPC-SO-39-No.456-2014**, realiza a través de videoconferencia, la sustentación de su trabajo de titulación denominado: **DESIGN OF A PILOT SCALE SAND FILTER TO EVALUATE THE COLOR REMOVAL CAPACITY OF IRON-TITANIFEROUS SANDS OF ECUADOR IN TEXTILE EFFLUENTS**, previa a la obtención del título de **PETROQUÍMICO/A.**

El citado trabajo de titulación, fue debidamente aprobado por el(los) docente(s):

Tutor	Dr. VILORIA VERA, DARIO ALFREDO , Ph.D.
Co - Tutor	Dr. RICAURTE FERNANDEZ, MARVIN JOSE , Ph.D.

Y recibió las observaciones de los otros miembros del Tribunal Calificador, las mismas que han sido incorporadas por el(la) estudiante.

Previamente cumplidos los requisitos legales y reglamentarios, el trabajo de titulación fue sustentado por el(la) estudiante y examinado por los miembros del Tribunal Calificador. Escuchada la sustentación del trabajo de titulación a través de videoconferencia, que integró la exposición de el(la) estudiante sobre el contenido de la misma y las preguntas formuladas por los miembros del Tribunal, se califica la sustentación del trabajo de titulación con las siguientes calificaciones:

Tipo	Docente	Calificación
Miembro Tribunal De Defensa	Dr. SOMMER MARQUEZ, ALICIA ESTELA , Ph.D.	10,0
Tutor	Dr. VILORIA VERA, DARIO ALFREDO , Ph.D.	10,0
Presidente Tribunal De Defensa	Dr. CAETANO SOUSA MANUEL , Ph.D.	9,9

Lo que da un promedio de: **10 (Diez punto Cero)**, sobre 10 (diez), equivalente a: **APROBADO**

Para constancia de lo actuado, firman los miembros del Tribunal Calificador, el/la estudiante y el/la secretario ad-hoc.

Certifico que *en cumplimiento del Decreto Ejecutivo 1017 de 16 de marzo de 2020, la defensa de trabajo de titulación (o examen de grado modalidad teórico práctica) se realizó vía virtual, por lo que las firmas de los miembros del Tribunal de Defensa de Grado, constan en forma digital.*

COBO ESPINOSA, JOSEPH ANDRES
Estudiante

Dr. CAETANO SOUSA MANUEL , Ph.D.
Presidente Tribunal de Defensa

MANUEL CAETANO SOUSA

Digitally signed by MANUEL CAETANO SOUSA
Date: 2020.09.30 15:34:50 -05'00'

Dr. VILORIA VERA, DARIO ALFREDO , Ph.D.
Tutor

Dr. SOMMER MARQUEZ, ALICIA ESTELA , Ph.D.
Miembro No Tutor

CIFUENTES TAFUR, EVELYN CAROLINA
Secretario Ad-hoc

AUTORÍA

Yo, **JOSEPH ANDRÉS COBO ESPINOSA**, con cédula de identidad 1804127296, declaro que las ideas, juicios, valoraciones, interpretaciones, consultas bibliográficas, definiciones y conceptualizaciones expuestas en el presente trabajo; así cómo, los procedimientos y herramientas utilizadas en la investigación, son de absoluta responsabilidad del autor del trabajo de integración curricular. Así mismo, me acojo a los reglamentos internos de la Universidad de Investigación de Tecnología Experimental Yachay.

Urcuquí, septiembre del 2020.

Joseph Andrés Cobo Espinosa
CI: 1804127296

AUTORIZACIÓN DE PUBLICACIÓN

Yo, **JOSEPH ANDRÉS COBO ESPINOSA,** con cédula de identidad 1804127296, cedo a la Universidad de Tecnología Experimental Yachay, los derechos de publicación de la presente obra, sin que deba haber un reconocimiento económico por este concepto. Declaro además que el texto del presente trabajo de titulación no podrá ser cedido a ninguna empresa editorial para su publicación u otros fines, sin contar previamente con la autorización escrita de la Universidad.

Asimismo, autorizo a la Universidad que realice la digitalización y publicación de este trabajo de integración curricular en el repositorio virtual, de conformidad a lo dispuesto en el Art. 144 de la Ley Orgánica de Educación Superior

Urcuquí, septiembre del 2020.

Joseph Andrés Cobo Espinosa
CI: 1804127296

This page is intentionally left blank.

To my Father and Mother, Patricio and Marisol,

and my whole family.

Acknowledgements

I would like to thank all the support that I have received from my supervisory committee. I would like to specially acknowledge Alfredo Viloria for allowing me to benefit from his previous experience. I thank the opportunity to learn from him during the academic courses taught by him, a teaching assistantship offered by him, and the enjoyable experience of working on my thesis project under his supervision. I truly appreciate his deep knowledge and the contribution to my maturity as a scholar and professional. I also want to thank all the professors who have contributed to developing my thesis for made me think critically at every stage of my project while providing sufficient guidance to go through my learning process and state my conclusions.

I'd like to thank my family for their support and motivation throughout my education. I'm truly in debt for my parents Patricio and Marisol, and my grandma Irma for allowing me to make all the academic opportunities possible.

Last but not least, I would like to thank all my friends and colleagues who have made my undergraduate experience much more pleasant and memorable.

Abstract

The textile industry is one of the most contaminants because of the heavy load of chemicals and dyes in the discharging effluents. The low biodegradability and high-water solubility of textile dyes lead to both environmental and economic concerns. Moreover, the high-efficiency dye removal from textile wastewater has been a challenge for many years. Several studies have been established adsorption and photocatalytic processes as promising dye removal treatment method. This study aimed to set up the sizing and design criteria required for a pilot-scale sand filter construction that enables to perform dye removal demo trials. Iron-titaniferous ecuadorian sand forms the granular filter material and decolorize textile effluents by performing the adsorption and photocatalytic process. The pilot-scale filter size is 1.59 m x 1.0 m x 1.05 m.

The sand filter was designed to handle 265 liters of textile wastewater per hour, and it was determined by analyzing the flow rate of the textile discharging effluents reported from the textile industries operated in Tungurahua province, Ecuador. The filter depth, flow control, and underdrain system allow accomplishing the backwashing and sand bed fluidization by uniformity up-flow water. The vertical and horizontal pressure exerted on the filter walls was calculated to determine the thickness selection criteria of the material for the sand filter construction. The sand filter design includes a weir and a small side tank to perform sand bed drainage and storage for further treatment or the final disposal.

This pilot-scale sand filter modular design may demonstrate a cost-effective device that is targeted to be performed and evaluated in situ in dye removal purposes from textile effluents of different textile factories. A simple, reliable, and economically feasible method to assess the dye removal effectiveness of the sand filter design is recommended.

Keywords: Sand filter, pilot-scale, dye removal, adsorption, photocatalytic process, and modular design.

Resumen

La industria textil es una de las más contaminantes debido a la gran cantidad de químicos y tintes textiles presentes en sus efluentes de descarga. La baja biodegradabilidad y alta solubilidad de los tintes textiles han creado preocupaciones medioambientales y económicas. Además, una alta eficiencia en la remoción de tintes del agua residual textil ha sido un reto por muchos años. Varios estudios han reportado resultados prometedores en la remoción de tintes textiles mediante procesos fotocatalíticos y de adsorción. Este estudio tiene como objetivo establecer el dimensionamiento y criterio de diseño para la construcción de un filtro de arena a escala piloto que permita realizar pruebas demostrativas de remoción de tintes textiles. Las arenas ferruginosas del Ecuador forman el material granular del filtro que decolorará los efluentes textiles mediante procesos de fotocatálisis y adsorción. El tamaño del filtro a escala piloto es 159 cm x 100 cm x 105 cm.

El filtro de arena está diseñado para tratar 265 litros de agua residual textil por hora. La capacidad hidráulica se determinó mediante el análisis de los efluentes de descarga reportados por las industrias textiles que operan en la provincia de Tungurahua, Ecuador. La profundidad del filtro, el control del flujo, y el sistema de drenaje permiten ejecutar el proceso de retrolavado y fluidización de la arena mediante la uniformidad de flujo en contracorriente. Se calculó la presión vertical y horizontal ejercida sobre las paredes del filtro para determinar el criterio de selección del material de construcción. El diseño del filtro de arena incluye un vertedero y un tanque pequeño que permiten el drenaje de la arena y su almacenamiento para tratamientos posteriores o su disposición final.

El diseño modular del filtro puede demostrar un equipo rentable que pretende evaluar la remoción de tintes presentes en los efluentes de diferentes empresas textiles. Se sugiere un método simple, confiable y económicamente factible para analizar la efectividad de la remoción de tintes del filtro de arena.

Palabras clave: Filtro de arena, escala piloto, remoción de tintes, adsorción, fotocatálisis, y diseño modular.

Table of Contents

List of Figures

List of Tables

Chapter I

Introduction

The textile industry is considered as one of the most significant users of water and complex chemicals during textile processes and also one of the major sources of water pollution. The amount of water used in textile processes varies widely and depends on the specific processes performed, the equipment used, and the prevailing philosophy of water use.[1] Ecuadorian textile industry is one of the second largest employment generators in the country and represents 7.5% of the entire industry in Ecuador. The textile industry contributes with more than 1040 million dollars to the national Gross Domestic Product (GDP).[2] Generally, the textile production stages are sizing of fibers, scouring, desizing, bleaching, washing, dyeing, printing and finishing. Regarding dyeing operation, it generates a significant percentage of the total wastewater.[3] Dyes are composed of atoms responsible for the dye color.[1] As the synthetic dyes provide a wide range of colorfast and bright colors, the fabric dyeing has become a massive industry today. [4,5] At present, the textile effluents are high in color, Biochemical Oxygen Demand (BOD), Chemical Oxygen Demand (COD), pH, temperature, turbidity, salinity, and toxic chemicals. [1,3,5–7]

Environmentalists have been concerned about the use and toxic nature of dyes as it causes adverse effects in the environment of life and various undesirable changes in the ecological status where the wastewater is directly discharged. The colloidal matter present in those effluents, along with colors, increases the turbidity and avoids the penetration of sunlight necessary for the photosynthesis process. Indeed, this fact interferes with the oxygen transfer mechanism at the air water interface, which in turn affects aquatic ecosystems by the toxicity of several dyes and their decomposition derivatives. Moreover, some studies have inferred that colored allergens may undergo biological and chemical assimilations, trigger eutrophication, consume dissolved oxygen, and avoid re-oxygenation in receiving streams. Hence, one of the greatest concerning effects of the direct discharging of this textile

wastewater into the environment or municipal treatment plants is the pollution of water and the adverse impact on flora and fauna. [1,4–6]

Even the direct discharge of the textile effluents into sewage networks produces disturbances in biological treatment processes performed in municipal wastewater treatment plants. These effluents cause a high concentration of inorganic salts, acids, and bases in biological reactors changing the environment of the microorganisms, which lies in increasing the wastewater treatment costs.[1,5,8] In this regard, the direct discharge of the textile wastewater into municipal sewage networks also produces adverse effects into municipal wastewater treatment plants. Dyes are part of the unused materials present in the textile effluents, and they have complex structures and high molecular weights resulting in low biodegradable molecules.[1] Thereby, the color removal is one of the most serious difficulties in dye wastewater treatment.

The dyes removal from textile effluents streams is ecologically necessary, and some environmental legislations obliges industries to remove the color from the dye-containing effluents before the disposal into water bodies.[7,9]

A separation process which may be used as a secondary treatment in wastewater treatment is granular filtration. The primary purpose of granular filtration is to remove filterable solids or suspended matter from water streams. Within water filtration, granular media, which is composed of granular particles, is usually used as the filtration medium. As granular filtration involves physical and chemical mechanisms, the media surface may be considered in adsorption purposes.[10,11] To illustrate, the adsorptivity of diatomaceous earth´s and clay may be applied in decoloring purposes.[12] Furthermore, Gomez[13] described the adsorptive and photocatalytic properties of the iron-titaniferous sand of Mompiche, located in the north-west coast of Ecuador. She reported the high decolorization percentage of crystal violet from water in a H_2O_2/UV system using the iron-titaniferous sands of Ecuador. Since the hydrogen peroxide (H_2O_2) is used in bleaching process,[14] the remmant H_2O_2 in the textile effluents can be reused. Thus, the high-efficiency rates in removing crystal violet dye from water may trigger industrial applications. As the crystal violet is a textile dye, one of those applications may be applied in decoloring purposes within the textile wastewater treatment. Biological

treatment and coagulation-flocculation processes are conventionally used in decoloring purposes within the textile wastewater treatment. However, coagulation dosages typically are not enough to achieve a significant removal of color when high levels are present.[15] Moreover, biological treatments like aerated lagoons are typically effective in biochemical oxygen demand (BOD) and suspended solids (SS) regulation but inefficient in color removal because of the low biodegradability and toxicity of textile dyes.[3,16]

Since the adsorptive and photocatalytic properties of the iron-titaniferous ecuadorian sands can be used in dye removal purposes,[13] the granular media in a sand filter may be considered for decoloring at the industrial scale. The challenge is to remove the remaining dyes from textile effluents before discharging.

Slow sand filters have shown a long history of success, and they are considered as substantial elements in water treatment plants. The proper functioning of these units requires a good design and adequate provision for maintenance. [17] In contrast to slow sand filters, rapid sand filters have been designed to operate at filtration rates of about 50 to 100 times greater than slow sand rates of filtration. [11,18] Thus, a slow sand filter can be designed and performed as tertiary treatment to remove dyes from textile effluents.

The pilot testing scale provides a reliable, low-cost method to evaluate a variety of treatment techniques without compromising the quality of the water in a real industrial process.[15] Hence, in this study, a pilot slow sand filter design is proposed to remove dyes from textile wastewater. The filter medium is composed of two filtration media layers: three graded gravel layers and sand bed. The iron-titaniferous black sands of Ecuador form the sand bed. Thus, the adsorptive and photocatalytic properties of the iron-titaniferous sands of Ecuador may be applied in industrial textile wastewater treatment applications. Thereby, starting from the crystal violet dye adsorption in ecuadorian black sands described by Gomez[13], an emerging technology may be performed in dye removal purposes to treat textile effluents.

As the sand filter will be focused on adsorption and photocatalysis processes only, the suspended solids must be treated previously. The pilot-scale sand filter is designed to handle 265 liters of textile wastewater per hour. To state this hydraulic loading rate, data of textile

effluents from the textile industry of Tungurahua province (Ecuador) was analyzed. Furthermore, the filter dimensions are 159 cm x 100 cm x 105 cm. Thus, one of the main advantages of the filter is to accomplish demo trials in different textiles factories. In other words, the filter can be operated with real textile wastewater, and it can be studied and analyzed in situ. The sand filter design comprises the sizing, analysis, and calculation of flow rate, filter area, filter medium, head loss, fluidization, triangular weir, underdrain system, filter depth, flow control, the pressure on the filter walls, selection of the raw material for the filter construction, and a recommendation for evaluation the dye removal effectiveness. The design criteria are also set up.

1.1   Objectives
1.1.1   General Objective

The general objective of this study is to design a pilot scale sand filter which allows dyes removal from the textile wastewater by exploiting the adsorptive and photocatalytic properties of iron-titaniferous ecuadorian sands.

1.1.2   Specific Objectives

- To determine the physical dimensions of the sand filter that enables to perform demo trials in different textile factories.

- To calculate and define the parameters and variables required for the filter modular design and construction.

- To set up the design criteria associated with the filter operation and sizing.

- To determine the hydraulic profile of the pilot-scale filter by calculating the loss of pressure and fluidization requirements for the backwashing process.

- To contrast the dye removal from textile wastewater by adsorption and photocatalytic process using the iron-titaniferous sands of Ecuador with the conventional decoloring methods.

Chapter II

Background Information

2.1 Iron-titaniferous black sands in Ecuador

Iron-titaniferous sands, also named ferruginous or black sands, are located in ecuadorian beaches, broadly in Guayas, Manabí, and Esmeraldas provinces. The presence of black sand deposits depends on not only the local conditions but also the presence of the parent rock, and they also can be from volcanic nature.[19] Ferruginous sands present a rounded structure due to wear as a result of waterway transport. Iron-titaniferous sands are composed of a natural mixture of minerals, which in high percentage present iron and titanium oxides. Usually, these minerals are magnetite (Fe_3O_4), ilmenite ($FeO \bullet TiO_2$), hematite (Fe_2O_3), rutile (TiO_2), zircon ($ZrSiO_4$), and silicates like quartz (SiO_2).[20,21] Associated metals such as manganese (Mn), magnesium (Mg), aluminum (Al), calcium (Ca), vanadium (V), chromium (Cr), and silicon (Si) also may be encountered.[22,23]

In the present, the black sands are used in the ecuadorian cement industry. The iron content present in the ferruginous sands increases the resistance of the cement. Furthermore, the iron metal may be obtained from the ferruginous sands. Additionally, the iron content can be used in the automobile and construction industry.[21,24] On the other hand, titanium dioxide can be obtained and used to produce paintings, paper, rubber, plastics, ceramics, surgical instruments, pieces for planes, coating for welding, and as a raw material for the titanium metal production.[22,24] Besides, the ecuadorian black sands may be used as a promising raw material for decoloring of textile wastewater.

2.2 Textile Wastewater

Wastewater may be defined as the water of a varied composition coming from the discharging of industrial, municipal, domestic, commercial, agricultural, and livestock uses. The contaminants present in wastewater embrace a mixture of organic and inorganic compounds.[25]

One important physical characteristic is color. Color in industrial wastewaters is associated with the presence of lignins, tannins, dyes, and other organic and inorganic chemicals. Color in water is classified in true color and apparent color.[26,27]

Apparent Color: Color is caused not only by substances in solution but also due to suspended matter. Apparent color includes the true color.[26,27]

True Color: Colloidal matter and suspended particles must be removed since they cause turbidity, which scatters and reflects light. Thereby, true color is the color in water which turbidity has been removed.[26,27]

2.3 Dyes

There is no information about the actual production of organic dyes in the world. However, it is known that more than 1000000 types of commercial dyes exist.[28] Dyes may be classified mainly in direct dyes (e.g. Direct red 28), vat dyes (e.g. Anthraquinone dye), azoic dyes (e.g. Naphthol AS), reactive dyes (e.g. C.I. Reactive red 3), acid dyes (e.g. C.I. Acid blue 113), disperse dyes (e.g. C.I. Disperse red 7), basic dyes (e.g. C.I. Basic violet 2).[29] In general, dyes are organic molecules that have two main functional groups in their molecular composition: (1) chromophores (responsible for the color), delocalize electron systems with conjugated double bonds just as $-C=N-$, $-C=O-$, $-N=N-$, $-N=O-$ and $-N=O_2-$ groups, (2) auxochromes (responsible for the color intensity), electron-donating substituent some of which are $-NH_2$, $-NR_2$, $-COOH-$, $-SO_3H$, and $-OH$ groups.[28]

2.4 Environmental Impact

One of the most difficult challenges faced by the textile wastewater treatment plants is the removal of color caused by dyes and pigments. These compounds are very resistant to biodegradation, and they may remain in the environment for an extended period. For instance, the half-life of the hydrolyzed dye Reactive Blue 19 (Figure 2.1) is about 49 years at 25°C and pH 7. [28,30,31]
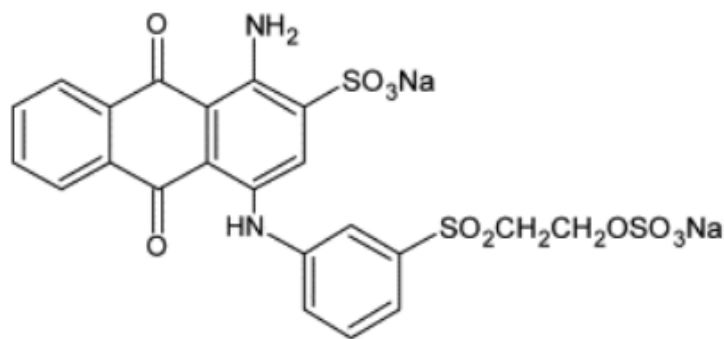
Figure 2.1. Illustration of a Reactive Blue 19 molecule.[32]

Most dyes used in dyeing and finishing operations are not removed in conventional wastewater treatment processes. They persist in the environment because of their high stability to light, temperature, detergents, and chemicals. The synthetic origin and aromatic structure make dyes resistant to biological degradation. The ingestion of water contaminated with textile dyes result in harm to human health and other living organisms due to the toxicity and mutagenicity of its components. Another important concerning about the presence of dyes in water is the decrease in light penetration and, consequently, photosynthetic activity. Also, oxygen deficiency limits the downstream to beneficial uses such as irrigation, drinking water, and recreational purposes. Furthermore, if dye-containing effluents are allowed to flow in the fields, it clogs the soil's pores resulting in loss of soil productivity. In this way, the soil´s texture gets hardened, and the penetration of plant roots is hindered. Even if the dye-containing effluents are discharged into the sewage systems, adverse effects are obtained. The dyeing-containing flow corrodes and penetrates the sewerage pipes and cause disturbances in biological treatment processes in municipal wastewater treatment plants. Besides, some of the organic material present in the textile effluents reacts with many disinfectants, particularly chlorine. The chemicals formed as products evaporate into the air and maybe inhaled or absorbed through the skin showing up as allergic reactions. [1,4,7,33] The general adverse effects of discharging textile effluents into the environment are outlined in Figure 2.2.
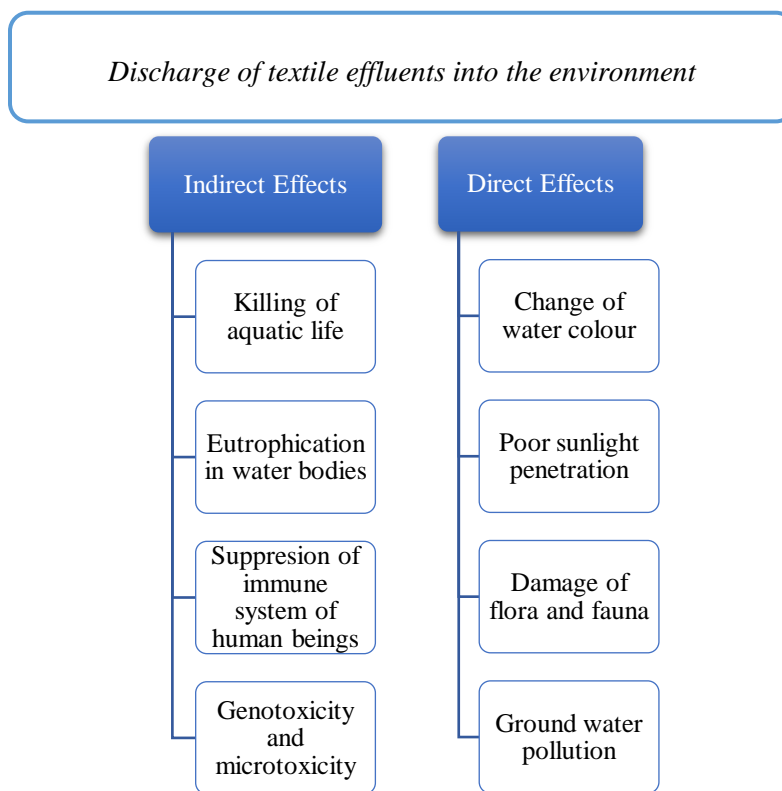
Figure 2.2. Effects of the discharge of textile wastewater into the environment. Taken from Verma[1].

2.5 Wastewater treatment

The treatment method required to treat wastewater lies in some regulations to be complied with before discharging. In general, wastewater treatment is classified in primary, secondary, and tertiary treatments. Primary treatment consists of removing solids in suspension and floating material. Secondary treatment encompasses conventional biological treatments. Regarding tertiary treatment, the main purpose is to eliminate contaminants that are not removed by primary or secondary treatments. Table 2.1 shows some processes performed in primary, secondary, and tertiary treatments.

Table 2.1. Conventional methods associated with primary, secondary and tertiary wastewater treatments.[25]

Primary Treatment	Secondary Treatment	Tertiary Treatment
Sedimentation	Activated Sludge	Filtration
Flotation	Aeration	Adsorption
Screening	Biological Filters	Chlorination
Neutralization	Anaerobic Treatments	Ozonation
Homogenization		Ionic Exchange
		Micro-sieving
		Reverse Osmosis

2.5.1 Treatment of Textile effluents.

Concerning the textile industry, effluent treatments may be classified into physical, chemical, and biological methods.[4] Table 2.2 shows several physical, chemical and biological treatment methods performed to treat textile effluents.

Table 2.2. Typical treatment methods classified into chemical, physical, and biological methods to treat textile wastewater.[4]

Physical Methods	Chemical Methods	Biological Methods
Sedimentation	Neutralization	Stabilization
Filtration	Oxidation	Aerated Lagoons
Flotation	Reduction	Activated Sludge
Coagulation	Catalysis	Anaerobic Digestion
Reverse Osmosis	Ion Exchange	Fungal Treatment
Solvent Extraction	Electrolysis	Flocculation
Radiation		
Adsorption		
Membrane Treatment		

A combination of different treatment methods may significantly remove unwanted matter. However, the treated effluent results high in color. Thus, a complimentary tertiary or decoloring treatment method is required to remove dyes with significant results.[4] The combination of wastewater treatment methods and one of the entire treatment processes used in the textile industry is illustrated in Figure 2.3.

2.5.2 Decoloring Methods in the Textile Industry

Biological and physicochemical methods usually are used to decolorize and degrade the organic compounds present in the textile effluents. There is no single economically and technically viable method to achieve the complete color removal from textile effluents in the world today. However, typically two or three treatment methods are combined with the ultimate purpose of achieving adequate levels of color removal. The common techniques are coagulation-flocculation, adsorption, and oxidation processes, which can be combined with biological treatments. Moreover, these technologies may also be combined with advanced oxidation or photocatalytic oxidation processes involving H_2O_2, ozone, and UV.[1,5,6,8,16] Other technologies are also performed (Table 2.3). Although all mentioned technologies may be efficient, most of them are expensive and provides further pollution, among other disadvantages (Table 2.4).

A)

B)
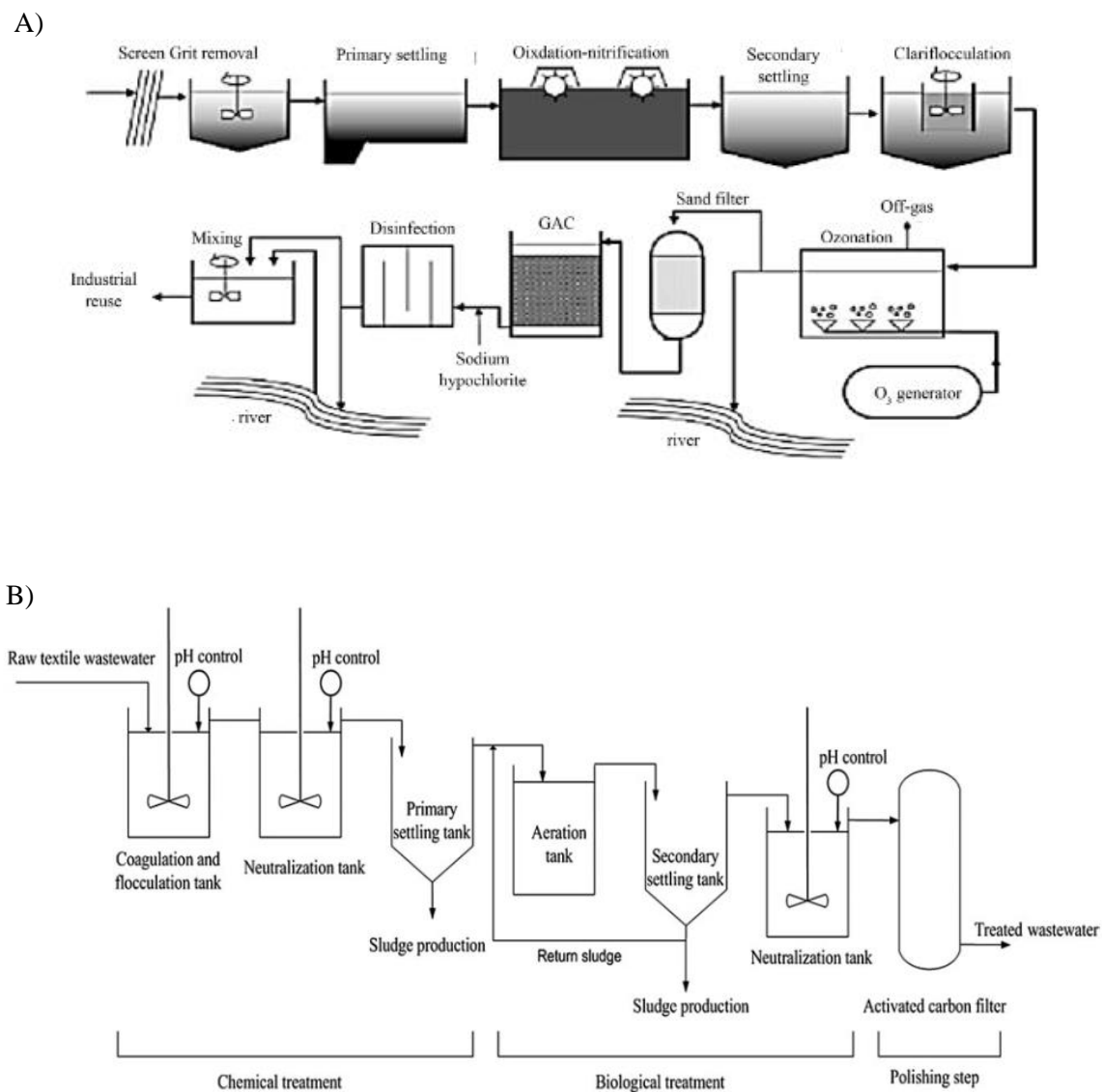
Figure 2.3. A) One of the conventional process-based treatment trial. [34] B) Dye wastewater treatment plant used by textile industries located at Kuala Lumpur.[28]

Table 2.3. List of Dye Removal Technologies.

TECHNOLOGY	DESCRIPTION
Ozonation	Oxidative process using ozone. The dosage depends on the total color to be removed with no sludge or residue generation. The volume of wastewater and sludge does not increase since ozone can be applied in a gaseous state. One of the main disadvantages is the short half-life, generally being 20 min. This time can be affected and even further shortened by the presence of salts, pH, and temperature. The drawbacks of this process mainly encompass the cost and continuous dosage.[35]
Photochemical process	Oxidative process using principally H_2O_2-UV. Besides, ultrasound is used to break chemical bonds producing free radical.[1,36,37]
Adsorption	Decolorization of textile effluents is carried out by adsorption. Solid supports are used to adsorb dyes on their surface area. [1,30]
Membrane Filtration	Dye removal from wastewater by physical separation. The selection of membranes lies in the pore size, membrane material, and membrane shape. Important problems such as high capital cost, the possibility of clogging, membrane replacement, and disposal of the residue left after separation must be considered. [1,35,38]
Ion Exchange	Cation and anion dyes may be removed from effluents by passing over the ion exchange resin. The process is performed until available exchange sites are saturated. Ion exchange is not entirely effective for disperse dyes, and it is associated with high cost.[35]
Electro-coagulation	Dye removal treatment based on electrodes (anode and cathode). Electrochemical oxidation efficiently remove color.[1,39,40]
Irradiation	Ionizing radiation treatment. Organic substances may be broken down by radiation in the presence of enough quantities of dissolved oxygen. [35]
Biological Process	Decolorization of textile effluents is achieved by microbiological degradation. Regarding microbial activity, a wide variety of microorganisms and several pathways are used.[1,35,41]
Chemical Coagulation and Flocculation	The addition of coagulants and flocculants may accomplish color removal from textile wastewater. The selection of coagulants and flocculants is governed mainly by the textile effluent´s characteristics like types of dyes, pH, organic contents, heavy metals, temperature. The large amount of coagulant agents and sludge generation is the major limitation of this process. [1,3,5]
Fenton Reagents	Advanced oxidation processes where H_2O_2 and Fe(II), UV with or without catalysis like TiO_2 are used. Highly reactive radical species are produced, circumstantially the hydroxyl radical (•OH) to react with dye molecules.[30,42]

2.5.2.1 Technology Depuration

Since the current available dye removal methods have described, a technology depuration can be accomplished with the final purpose of establishing the real cost-effective technologies which may be implemented at industrial scale for that purposes. Regardless of the advantages and disadvantages of the dye removal technologies, to state a promising process that may be implemented in real textile wastewater treatment, three criteria concerning efficiency, affordability, and dosage of a chemical or biological compound are considered (Table 2.5).

Table 2.4. Advantages and disadvantages of particular methods used in dye removal of textile effluents.[1,28,35,36]

Physical-chemical methods	Advantages	Disadvantages
Ozonation	Application in a gas state	Short half-life High cost
Photochemical process	No sludge production	Formation of secondary pollutants High Cost
Adsorption	Exceptional removal of a wide variety of dyes	Regeneration difficulties Costly disposal of adsorbent Sludge generation
Membrane Filtration	Physical separation	Removal of all types of dyes
Ion Exchange	Easy regeneration	Not useful for all dyes
Electro-coagulation	Good removal of dye	High cost
Irradiation	Effective oxidation at lab scale	Not effective for all dyes High cost
Biological treatment	Environmentally Friendly	Slow process Narrow operational temperature range Nutrients required
Chemical coagulation and flocculation	Excellent color removal Economically feasible	High cost of chemical reagents Sludge generation
Fenton reagents	Effective decolorization of soluble and insoluble dyes	Costly chemical reagents Generation and handling of sludge

Table 2.5 Criterion to be considered in the dye removal technology's depuration.

Criterion 1	High Efficiency
Criterion 2	Economically Feasible
Criterion 3	No chemical or substrate dosage required

Table 2.6 illustrate the fulfillment of the established criteria in each dye removal technology described in Table 2.5. It is observed that the adsorption and the photocatalytic process by iron-titaniferous ecuadorian sands at first instance meet the three established criteria stated in Table 2.5. Besides, the parameters showed in Table 2.7 may be considered to build a real perspective about the performance and implementation of any technology focused on dye removal purposes for textile effluents. Then, the weighing of each parameter may be carried out by analyzing survey responses of professionals associated with each parameter section. It can be developed by an expert opinion matrix. The final decision to implement, develop,

and perform a dye removal technology in real wastewater treatment depends on the analysis of the results provided by the expert opinion matrix.

Table 2.6 Comparison of the fulfillment of the established criteria by each dye removal technology.

Technology	Criterion 1	Criterion 2	Criterion 3
Ozonation	✓	✗	✗
Photochemical process	✓	✗	✗
Conventional Adsorption	✓	✗	✓
Membrane Filtration	✓	✗	✓
Ion Exchange	✗	✗	✓
Electro-coagulation	✓	✗	✗
Irradiation	✗	✗	✗
Biological Treatment	✓	✓	✗
Chemical Coagulation and Flocculation	✓	✓	✗
Fenton Reagents	✓	✓	✗
Adsorption and photocatalytic process by iron-titaniferous ecuadorian sands	✓	✓	✓

2.5.3 Conventional Dye Removal Treatments

2.5.3.1 Technology I: Coagulation-Flocculation

Chemical coagulation-flocculation is observed as one of the most practiced technology in decoloring purposes and suspended particles removal. This method provides excellent color removal since most of the dyes used in the textile industry may be removed. However, the mechanism of coagulants applied to decolorize textile effluents is still not definitively clear. Coagulation of dye-containing effluents has been practiced for many years as principal treatment or pretreatment because of its low cost. Nevertheless, this method's main limitation is the high chemical dosage of coagulating agents, the generation of sludge, and the deficient decolorization of several soluble dyes. The coagulation-flocculation process often is combined with other techniques such as biological treatments to achieve an acceptable effluent color quality.[1,3,5,30]

Table 2.7. Parameters to consider in the dye removal technology performance.

Technical Parameters

- Regeneration
- By-products generation
- Sludge generation
- Testing operational conditions
- Flow fluctuation flexibility
- Pretreatment requirement
- Chemical dosage requirement

Constructability parameters

- Special services requirements (e.g., pumps, valves, piping, underdrain, or backwash system)
- Area required for construction
- Expansibility
- Process and instrumentation diagram
- Coverage

Operational parameters

- Number of cycles
- Flow control
- Temperature-sensitive
- pH-sensitive
- Residence time
- Electricity consumption
- Overflow
- Hydraulic loading rate

Maturity parameters

- Risk and Maturity of the technology
- Years in operation

Availability parameters

- The raw material for dye removal availability
- The raw material for construction availability

Economic Parameters

- Construction cost
- Raw material cost
- Operational Cost
- Final disposal treatment cost
- Maintenance cost
- Operators cost

Strategic/Geopolitical parameters

- Regulations by law
- Innovation

Environmental parameters

- Environmental impact
- Environmental regulation

Various inter-related parameters are involving in the coagulation process as it is a complex phenomenon. Thus it is very critical to determine what is the performance of a coagulant under given conditions.[1] In chemical coagulation, chemical coagulants can be categorized in hydrolyzing metallic salts, pre-hydrolyzing metallic salts, and synthetic cationic polymers. Another categorization based on natural coagulants can be considered: plant-based, animal-based, and micro-organism based coagulants. The conventional coagulants used in the textile industry are aluminum sulfate (Alum), ferrous sulfate, ferric chloride, and ferric chloro-

sulfate. The mixing speed and time, temperature and retention time, and pH are the most critical parameters to be considered as they influence the efficiency of color removal.[1,5]

The significant innovations in dyes synthesis with complex structures provide difficulties in the selection of the proper coagulant. Therefore, different types of dyes required a re-evaluation of the optimum conditions for the coagulation process.[1]

It is essential to mention that the disposal of the sludge generated during the coagulation-flocculation process is problematic and expensive. In this way, several studies related to the use of the sludge as a building material or soil conditioner have been carried out.[1]

In short, coagulation-flocculation methods have some advantages as well as certain drawbacks, and their selection is mostly governed by textile effluent's characteristics like types of dyes, pH, organic contents, heavy metals, temperature, etc. Although coagulation-flocculation is generally practiced by the small to large scale industries, it is even being a cost-comparative alternative for the treatment of textile effluents.[1]

Several studies in coagulation-flocculation have been carried out to find the highest efficiency in color removal. To illustrate, synthetic and biodegradable polymeric coagulants such as cyanoguanidine-formaldehyde[5], a combination of inorganic coagulants and synthetic polymeric[5], polyamines as flocculants[5], composite flocculants[3], polyferric sulfate[43] have been performed as coagulants with color removal purposes.

2.5.3.2 Technology II: Adsorption by Activated Carbon

Since this method has been efficient in decoloring textile effluents, adsorption processes provide good quality effluents with a low concentration of dissolved organic compounds such as dyes. However, this technology is limited by the high cost of the adsorbents.[9,16]

Regarding the sorption process, temperature, adsorbent dose, pH, and contact time values are established to obtain the equilibrium isotherms. These isotherms are generally based on the Langmuir and Freundlich models to study the adsorption capacity of adsorbents.[9,16]

Low-cost materials from industrial waste to agricultural products have been performed in adsorption processes to reach cost-effective dye removal technology.[16] For instance, peat[44,45], bagasse pitch[46], Fuller´s earth[47], lignite[48], coal[49], alum sludge[50], bagasse fly ash[51], perlite[52], silica[53], coir pitch activated carbon[9], polymer and mineral sorbents[8] have been studied but they require further research.

Activated carbon may be considered as the most common adsorbent and may be very effective for several dyes. Activated carbon developed from bamboo, fertilizer waste, activated carbon fiber, and coconut shell fibers have shown promising results. However, the adsorption by activated carbon still prevails as an expensive process.[1,16] Furthermore, the major problem related to the adsorbents are the regeneration and recovery of the useful material which is unattractive for commercial applications.[16]

2.5.3.3 Technology III: Dye removal by iron-titaniferous ecuadorian sands

Gomez[13] described the adsorptive and photocatalytic properties of the black sand of Mompiche beach, located on the north-west coast of Ecuador, and Quilotoa volcano sand from the ecuadorian Andes. These ferruginous sands were sampled, named and characterized by Vera[54]. An adsorption and photocatalysis integrated process was performed to study the crystal violet removal effectiveness in the ecuadorian ferruginous sands. The most influential variables in this process are irradiation, the type of catalyst, time of reaction, temperature, pH, and hydrogen peroxide concentration. The sand of Mompiche beach (SEM-205) and sand of Quilotoa volcano (SXQ-102) were studied and shown a very high discoloration percentage under pH 8, hydrogen peroxide (1M), and UV irradiation. The kinetics of the crystal violet discoloration by SEM-205 and SXQ-102 is illustrated in Figure 2.4 and Figure 2.5.
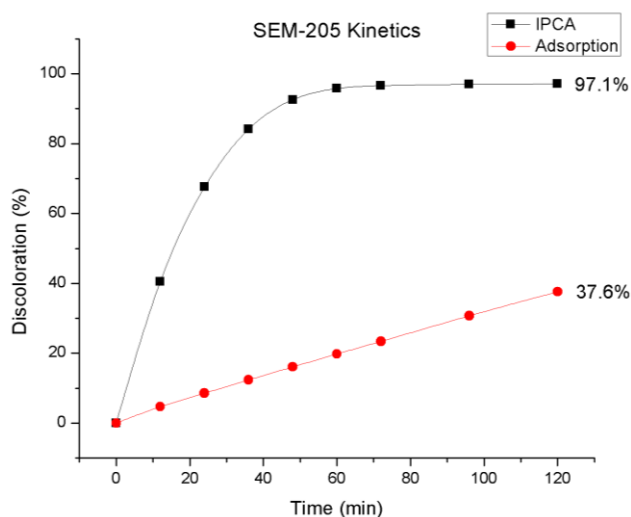
Figure 2.4. Kinetics of Crystal Violet discoloration by Mompiche sand (SEM-205).[13].
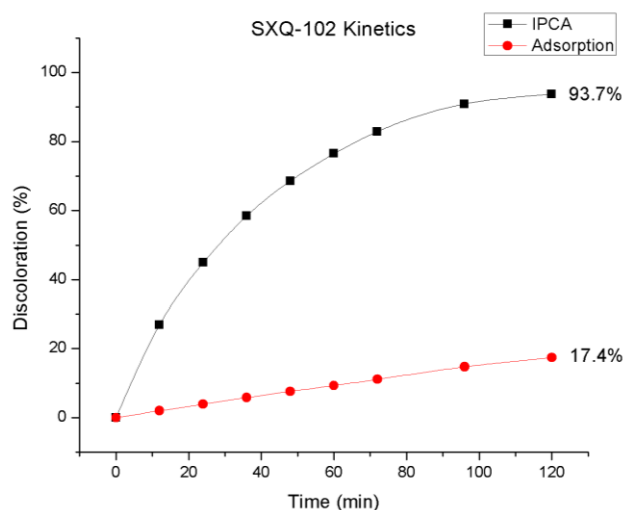
Figure 2.5. Kinetics of Crystal Violet discoloration by Quilotoa sand (SXQ-102).[13]

After two hours, SEM-105 reaches the highest discoloration percentage. At first instance, the slope of the discoloration can be interpreted as the discoloration velocity. Thus, the slope of the SEM-105 kinetics shows a higher discoloration velocity as compared with SXQ-102. In other words, it can be observed that Mompiche sand (SEM-105) remove a higher percentage of dye in a shorter period than Quilotoa sand (SXQ-102).

The high-efficiency rates in removing crystal violet dye from water may trigger industrial applications. Since crystal violet is one of the most used dyes in the textile industry and based

on the promising results reported by Gomez[13], an emerging technology may be developed in dye removal purposes to treat textile effluents. To illustrate, an S-curve is used to present the natural growth pattern of a new technology (Figure 2.6). In other words, the S-curve reflects the evolution of a technology performance, and it is divided into three sections. The lower part of the S-curve pertains to the innovation stage, and it is associated with the exploration or researching at the lab scale. The middle part of the S-curve relates to the growth stage, and it is associated to the experimentation or field test. Finally, the upper part of the S-curve pertains to the maturity stage, and it is correlated with the exploitation or the adoption of the new technology.[55–57]
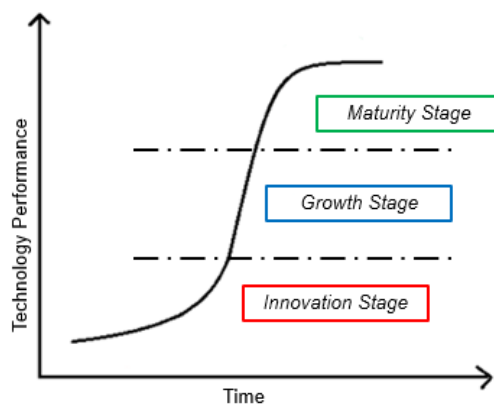
Figure 2.6. The S-curve model of an emerging technology.

Thus, the Mompiche (SEM-205) sand may become a promising raw material to perform cost-effective adsorption and photocatalytic process in dye removal treatment for textile wastewater. Since the Mompiche sand is a granular material, the most convenient and cost-effective method to perform the integrated adsorption and photocatalytic process is using a granular filter.

2.6 Granular Filters

Granular filtration is one of the most conventional methods used to remove colloidal, or suspended contaminants from water. The granular filtration process commonly consists of a filter box in which a granular bed is placed on a support layer with an underdrain mechanism at the bottom. Several configurations such as media type, filtration rate or hydraulic loading rate, backwashing system, filtration rate control, and even the pretreatment level are

considered to describe granular filters. In general, the filter's classification encompasses three different types according to the force which forces the water to pass through the filter.[10,15,17]

- Gravity filters
- Pressure filters
- Up-flow filters

Usually, two types of granular filters are typically performed: slow sand and rapid sand filters. These filters are classified and differentiated mainly by their filtration rates. Slow and rapid sand filters operate at slow-rates and high-rates of filtration, respectively. The filtration rate may be defined as the superficial water velocity through the filter bed, and it can be calculated by the ratio of the flow rate and the cross-sectional area of the bed. [10,11,17,58] The filter bed is composed of a porous medium. This medium consists of granular particles where indivisible grains rest on each other. Sand, anthracite, coal, garnet, and ilmenite are commonly used in the filter medium. The adsorptive characteristics of the medium may be approached to remove the chemical contaminants from wastewater streams. [11,12,59] Granular medium may have different media composition and arrangement, and media size distribution. From this point, some properties such as grain size, shape, density, bed porosity, hardness, and specific surface area can be considered.[10,11]

2.6.1   Granular Medium Specifications

2.6.1.1 Grain size distribution

As the grain size distribution affects the hydraulic performance of the filter, it is essential to select the correct design criterion to achieve an effective hydraulic performance. Thereby, it is important to mention that small grain sizes tend to produce high head losses, while large grain sizes tend to produce lower head loss values. The grain size distribution is determined by sieving. Regarding sieving analysis, the sieves are placed in ascending order with the largest opening on the top and the smallest opening on the bottom. Then, a sample is placed on the top sieve, and the rack is shaken for an established amount of time. The mass of material retained on each sieve is determined at the end of the shaking period. Hence, the

cumulative mass is recorded and then expressed into percentages. Effective size ranges for slow sand filters varies between 0,25 mm. to 0,35 mm even when conventional fixed bed filters use the granular medium of 0.5 mm. to 1 mm. in size.. [17,58,60]

2.6.1.2 Hardness

The hardness of the filter material expresses the resistance to abrasion and breakdown produced during the filter backwashing. The Moh scale represents the hardness in the range between 1 to 10, and design specifications should establish minimum specified values to avoid excessive abrasion. Sand, garnet, and ilmenite withstand the abrasion significantly, but anthracite and activated carbon are considered friable. The typical value in the Moh scale for sand is 7.[11,17]

2.6.1.3 Porosity

It is also termed as a void fraction. It can be defined as the space between grains expressed as a fraction of the total filter bed. Porosity has a significant influence on head loss during filtration.[11,59] It can be determined by equation 1.

$$\varepsilon = \frac{V_v}{V_T} \qquad\qquad (\ 1\ )$$

Where,

ε = Porosity (Dimensionless)

V_v= Volume of voids in a granular bed (m^3)

V_T= Volume of media (m^3)

2.6.1.4 Specific Surface Area

The specific surface area of a filter bed is explained as the total surface area of the filter material divided by the filter bed volume.[11]

2.6.1.5 Effective size

The effective size is determined by sieve analysis, and it is defined as 10% of the medium that presents a smaller grain size. In other words, it is the sieve opening in which 10% of the finer medium passes through. The effective size considered for slow sand filters ranges between 0.25 mm. to 0.35 mm.[11,18,58]

2.6.1.6 Uniformity Coefficient

The uniformity coefficient's primary purpose is to characterize the fine and coarse grain distributions in the filter media. Small grain sizes tend to cause higher head losses, while large grain sizes tend to produce small head losses. Since the filter medium is never uniform, the grain sizes are specified in terms of effective size or uniformity coefficient. It is determined by sieve analysis as the ratio of the size of the sieve opening in which the 60% finer of the medium pass-through (S_{60}) to the size of the sieve opening in which the 10% finer of the medium can pass through (S_{10}). In short, the uniformity coefficient is the ratio of (S_{60}) divided (S_{10}). [10,18,58] The uniformity coefficient of the granular material used in slow sand filters ranges between 2 to 3.[18,58]. However, the uniformity coefficient suggested for sand bed ranges between 1.3 to 1.8.[11]

2.7 Slow Sand Filters

Low capital cost, easy operation and maintenance, filtered water quality, and short construction periods may be considered as important criteria related to the selection of the type of filter. The system referred to slow sand filters may be regarded as simple, reliable, cost-effective, and easy to build and operate. In this way, highly trained operators are not required. Furthermore, minimal power requirements during the filter performance are needed.[18]

As undesirable impurities may be encountered in the sand, the sand bed must be free of clay, dust, and other impurities.[12] Moreover, if the loading raw water contains a significative amount of suspended matter, the coagulation-flocculation pre-treatment process is required previous slow sand filtration process. [12]

Slow sand filtration with adsorption purposes must be preceded by a pretreatment process to reduce the suspended solids load in the filter. Thereby, often flocculation and coagulation precede granular filtration. Then, the adsorption and photocatalytic process's efficiency may be limited by some physical characteristics of the filter bed, and the effectiveness of pretreatment. [12,18]

2.7.1 Slow Sand Filter Criterion Design

Fundamentally, the main structure of a slow sand filter consists of a tank that contains a supernatant layer of raw water, a filter bed, an underdrain mechanism, an outlet and inlet structure, and a set of filter regulations and control devices. The supernatant water layer provides a sufficient head of water, which drives the raw water through the filter bed and creates a certain period of time for the raw water. Regarding the filter bed, fine sand is the main component. The underdrain mechanism's primary purposes are to allow the treated water flows to the outlet structure and support the filter medium.[61]

According to Kawamura[18], some items must be determined before designing a filtration system. The items selection is based on local conditions, regulatory constraints, plant capacity, quality of raw water, type of treatment process, possible head loss across the filter, and potential for future expansion and/modification. The main items to establish are:

2.7.1.1 Loading Rate

The loading rate may be defined as the water flow rate charged into the unit area of the filter bed. Furthermore, it shows the same value of the flow velocity approaching the surface filter. The criterion design provided by Mackenzie[17] is that the water may be applied to the sand at a loading rate of 0.13 to 0.33 m/h. Conventionally, the hydraulic loading rate used as an effective design criterion is 0.15 m/h.[60,62] The hydraulic loading rate may be determined by equation 2.

$$LR = Q/A \hspace{3cm} (\ 2\ )$$

Where,

LR= Loading Rate (m/ h)

Q= Flow rate (m/ h)

A= Surface Area of the filter (m^2)

2.7.1.2 Filtration Rate

The filtration rate specifies the flow rate through the filter divided by the bed's surface area, and it typically presents volumetric units. The selection of filtration rate and head loss for a particular type of filter and filter medium may be dictated by the total required area of the filter bed, the available hydraulic head loss across the filter bed, the terminal turbidity breakthrough in the filter bed, and the length of the filter run.[11,18,58] Valves in the effluent piping usually control the flow rate and the filter level. In an outlet-controlled filter, the filtration rate is established by the outlet valve. If the flow resistance across the filter bed increases, the valve has to be opened a little further to maintain the established filtration rate. On the other hand, valves also can be located at the inlet of the filter. In an inlet-controlled filter, the filtration rate is set by the inlet valve, and no further manipulation is needed. Thus, the filtered water flow rate can be controlled by the adjustment of an effluent drain valve.[63] Furthermore, filtration rates can be judged two variables: the quality of the water produced and the length of the filter run. In filtration process for decoloring purposes, the water quality may be expressed by a profile turbidity.[10,15,61]

2.7.1.3 Hydraulics

Issues associated with the hydraulic performance may be encountered during the sand bed adsorption and photocatalytic process. In this regard, head loss (loss of pressure) through a clean filter bed and head loss due to the deposited materials must be considered. Several and well-known equations have been performed to describe the head loss, but most of them are limited to clean filters. There is no method to predict the increase of the filter head loss without full scale or pilot plant filter data. Besides, the experience and the hydraulic profile

provide an accurate head loss development during a filter run.[15,17,58] The rate of increasing in head loss during a filter run is proportional to the rate of solids retained by the filter. [15]

2.7.1.4 Filter Size and Filter Area

The filter size selection lies in the uniform flow distribution of the backwash water over the whole filter bed, the economically feasible size of the filter backwash tank and pumps, and the cost of the handling facilities related to the backwash.[18] The filter area is determined by the expected flow rates and the selected design unit flow rate. The entire filter box dimensions are commonly limited by the backwash requirements such as storage, recovery, and the backwash rate.[10]

2.7.1.5 Filter Medium

The filter medium can be composed of monomedia or multimedia of any granular material, depending on the purpose. One condition of the filter bed is that the coarser heavy grains are placed at the bottom of the filter. Silica sand and anthracite coal are typically used as a filtration medium. Other materials such as garnet, ilmenite, pumice, and synthetic materials may be used as filtration media, but their availability and cost limit them. Generally, due to its availability, low cost and durability, fine sand as filtration media are applied to slow sand filters, it also provides simple design and construction. Besides, sand must be free form clay, soil, and organic matter before placed into the filter. [18,58,61]

2.7.1.6 Filter Depth

Filter depth is measured from the underdrain supporting slab to the top of the filter wall. The filter depth criterion design is settled depending on media depth, underdrain design, and the freeboard. It is important to point out that freeboard is required and determined by the hydraulic profile.[10]

2.7.1.7 Filter Support

The underdrain system requires a gravel support bed depth ranging from none to several gravel gradations. The filter bed is poured onto gravels of increasing permeability.

Conventionally, the thickness of each layer is about 10 to 25 cm. The gravel's size ranges from 18 to 36 cm. These sizes may be gradually diminished, ranging from 10 to 12 cm or less for the upper filter support layer. [10,12]

2.7.1.8 Underdrain System

The layer/s forming the filter bed has to be supported by the underdrain mechanism. As the water flows in a downward direction, underdrain system's essential purpose is to allow the filtered water to be drawn off while the filter medium is retained in place. Another fundamental role of the underdrain system is to distribute uniformly the backwash water through the filter bed during the backwashing process. Three major underdrain systems may be described. First, the standard and oldest type is the manifold-lateral system in which perforated pipe laterals are located at intervals along a manifold. Thereby, the filtered water passes through perforated pipes into the filter effluent piping (Figure 2.7). As criterion design, perforations in the laterals are placed on 8 to 30 cm spacing, and they are between 6 to 13 mm. Second, a fabricated self-supporting underdrain system is attached to the filter floor (Figure 2.8). To illustrate, vitrified clay block underdrain and plastic block underdrains may be used. As a design parameter, the top openings of this underdrain are about 6 mm. when gravel support is used. Third, a false-floor (slab or steel may be used) underdrain with nozzles may be performed. The false-floor is placed 0.3 to 0.6 m. above the filter's bottom, they are hence providing an underdrain plenum below the false-floor. The role of the nozzles is to collect the filtrate and distribute the backwash water during backwashing. As a criterion design, nozzles are located at 13 to 20 cm centers and they may have coarse openings (of about 6 mm) or fine openings, small enough to retain the filter media (Figure 2.9).[12,15,58] The loss of pressure through the underdrain becomes critical if the filtration rate is increased significantly.[10]
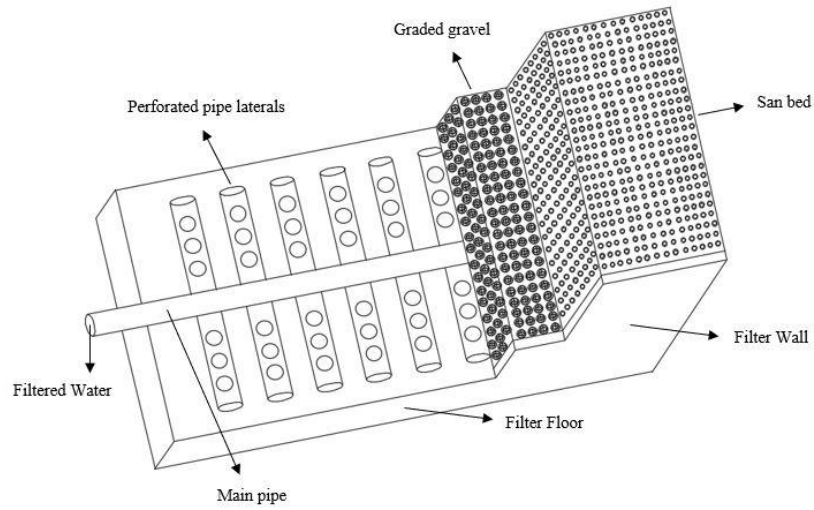
Figure 2.7. Sand bed filter with a manifold and perforated pipe laterals underdrain system.
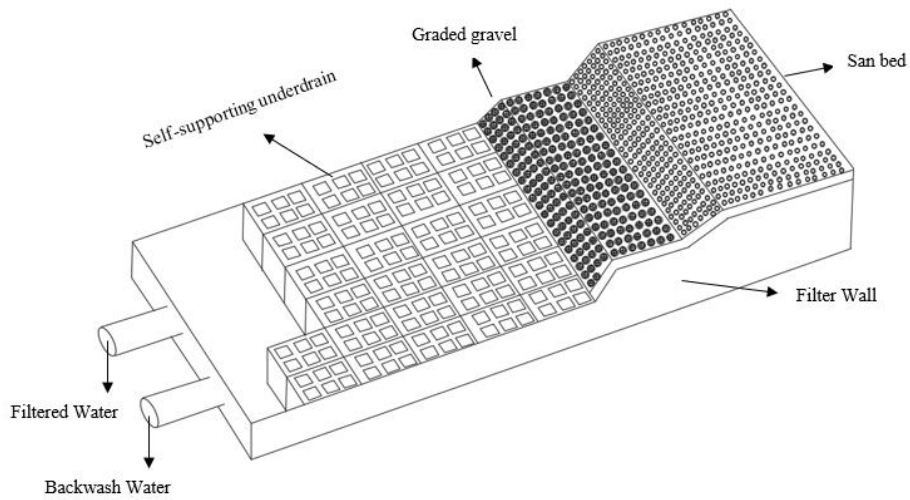
Figure 2.8. Sand bed filter with a self-supporting block underdrain system.
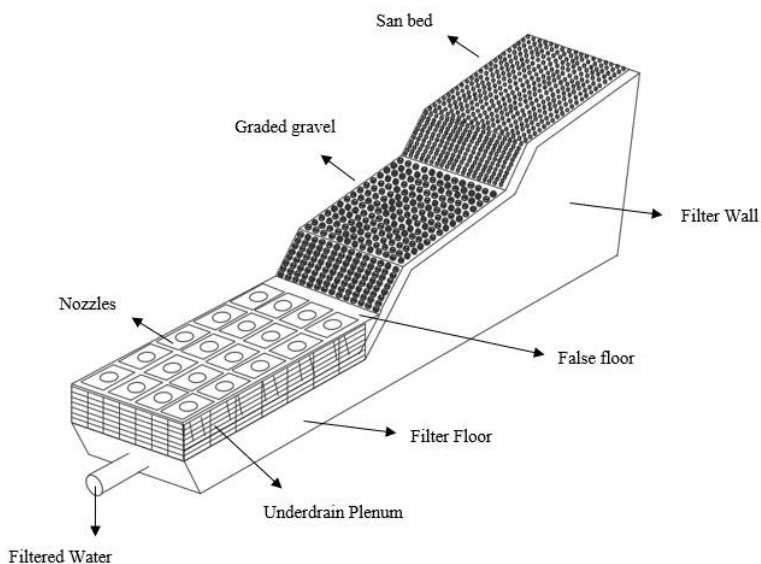
Figure 2.9. Sand bed filter with a nozzle underdrain system consisting of a false-floor slab with nozzles capable of air and water distribution.

2.7.1.9 Flow Control

Filters usually suffer changes in the flow rate since, commonly, the total plant flow is not constant, which could affect the filtration quality. Flow control can typically be divided into mechanical control and non-mechanical control systems to achieve the hydraulic flow control in the operating filter.[15] As mentioned before, valves in the effluent piping usually control the flow rate and the filter level. In an outlet-controlled filter, the filtration rate is established by the outlet valve. On the contrary, valves also can be located at the inlet of the filter. In an inlet-controlled filter, the filtration rate is set by the inlet valve, and no further manipulation is needed.[10,15,61]

2.7.1.10   Filter Floor

Conventionally, the sand and graded gravel rest on a concrete floor.[58] Nevertheless, the floor depending on the raw material selected for the filter construction.

2.7.1.11   Backwash System

The backwashing operation's main purpose is to remove solids deposited into the filter media and return a clean condition. Furthermore, the filter must be backwashed to avoid the

turbidity breakthrough, and it is determined by experience. Hence, the selection, design, construction, and operation of the backwash system play a key role in the adsorption and photocatalytic process. Generally, the backwashing process consists of introducing a flow rate of clean water at the filter underdrain with a velocity capable of expanding the bed. [10,15,58] Two alternatives to backwash methods are compared in Table 2.8.

Table 2.8. Backwash alternatives for granular bed filter.[15]

	Backwash Method	
	With Fluidization	Without Fluidization
Applications	Fine sand Dual media Triple media	Coarse single-media sand or anthracite
Fluidization	Yes, during water wash	No
Bed Expansion	15-30 percent	Negligible
Wash Throughs	Typically used	Usually not used
Horizontal water travel to overflow	Up to 0.9 m.	Up to 4 m.
Vertical Height to Overflow	0.76 – 0.91 m.	0.6 m.

2.7.1.12   *Expansion of Filter Media during Backwashing*

The expansion of the bed avoids clogging by dislodging clogging materials. The filter bed may expand about 15 to 30 percent above its fixed bed depth when the backwash up-flow causes the fluidization of the bed. The bed expansion is affected by several variables associated with the filter medium and the water. The variables related to the filter media include the size, grain shape, size gradation, and density. Water variables lie in viscosity and density. To expand the filter bed, the backwashing force acting upward upon the column of water must be equal to the pressure at the bottom of the filter. [15,58]

2.7.1.13   *Freeboard*

The freeboard is defined as the physical space provided above the filter bed to allow its expansion during backwashing[12], and it is required by the hydraulic plant profile.[10]

Chapter III

Design Methodology and Sizing

3.1 Flow rate (Q_o)

Relevant information about textile effluents from the textile industries operated in Tungurahua province, Ecuador, has been provided by The Management and Environmental Quality Department of Ambato city. Tungurahua is one of the provinces with the highest number of textile factories in Ecuador.[64] The data primarily contains the discharging flow rate of these factories of fabrics and textile finishing (see Appendix A). Fundamental statistical analysis of maximum and minimum reported discharging flows of these factories have been performed. Conventionally, each factory of fabrics and textile finishing should report the maximum and minimum discharging flow. However, the maximum discharging current has been reported by sixty-four factories, and the minimum discharging flow has been reported by thirty-six textile factories of seventy-three textile factories operated in Tungurahua. These values are shown in Appendix A (Table A.1), pH is also reported. The pilot-scale filter design in this study is targeted to perform demo trials. It means the filter may be operated, evaluated, and analyzed in situ with real textile effluents from the real textile industry. Table 3.1 shows the MODE (Q_M) of the maximum and minimum discharged reported flows. In this context, the mode is defined as the value that occurs most often in a data set.[65]

Table 3.1. Mode of the maximum and minimum discharging flow reported by textile factories operated in Tungurahua.

Maximum Discharging Flow	
$Q_{M\,max}$ (l/h)	5292
Minimum Discharging Flow	
$Q_{M\,min}$ (l/h)	4320
$Q_{max} = Q_{M\,max} \times 5\%$	
Q_o (l/h)	265

In other words, the mode is defined as the most reported maximum and minimum discharging flow. Since the pilot-scale sand filter is targeted to be evaluated and performed in different

textile factories, the hydraulic loading rate will be five percent (5%) of the most reported effluent by the Tungurahua's textile industries (Q_o). It means that the inlet flow of the pilot-scale filter will be five percent of the MODE of the maximum discharging flow. Thus, the modular design also considers an ease transportation pilot-scale sand filter.

3.2 Filter Box Sizing

Since the hydraulic loading rate of the filter is established, filter area can be defined as the volume of fluid passing through a given cross-sectional area per unit time. The time to allow the loading rate to pass through the filter area is stated as 0.75 h. This variable is supported by observing the kinetics of the photocatalytic-adsorption process reported by Gomez[13] (Figure 2.4). The kinetics shows that Mompiche ecuadorian sand has achieved approximately 80% of the discoloration of crystal violet in 30 min. With this in mind, one may expect a half-hour as the targeted time to perform a dye removal process in an industrial process. However, an overdesign factor (50%) is considered to counteract any disturbance in the adsorption-photocatalytic process. Then, the equation 3 can be applied to find the volume of the filter.

$$Q_o \ (\text{m}^3/\text{h}) = Vol \ (\text{m}^3)/t \ (\text{h}) \qquad\qquad (3)$$

Where,

Q_o = Inlet flow rate in the filter per unit time (m^3/h)

Vol = Volume of the filter (m^3)

t = Expected time to let the inlet flow rate to pass through the filter. (h)

The real volume where the raw water passes through is the bulk void fraction of the filter medium. The bulk void fraction is expressed as the porosity of the medium. Since the iron-titaniferous sands of Ecuador perform the adsorption-photocatalytic process, only the sand media is considered for the design analysis. Then, the filter volume is obtained using the equation 4.

$$Vol \ (\text{m}^3) = (Q_o) \ x \ (\varepsilon) \ x \ (t) \qquad\qquad (\ 4 \ )$$

Where,

Vol = Filter volume. (m^3)

Q_o = The MODE of the maximum discharging flows of the Textile industry of Tungurahua. (m^3/h)

ε = The space between grains (void fraction) of the Mompiche sand (SEM-205)

t = Expected time to let the inlet flow rate to pass through the filter. (h)

Once the volume is determined, it can be defined as equation 5.

$$Vol \ (\text{m}^3) = A \ x \ h \qquad\qquad (\ 5 \ )$$

Now, the filter area (A) and the sand bed height (h) are calculated by using optimization techniques. The filter volume Vol (m^3), filter Area (m^2), and sand height (m) are reported in Table 3.2.

Table 3.2. Filter Volume, filter area, and sand height.

Vol (m^3)	0.20
h (m)	0.30
A (m^2)	1.59

Then, the filter area A is defined as equation 6.

$$A = \ S_1 \ x \ S_2 \qquad\qquad (\ 6 \ )$$

Where S_1 and S_2 are the filter length and the filter width conforming the filter area.

Since the filter is targeted to be at a pilot scale, a rectangular form is considered. In this way, a ratio between the length and width of the filter must be calculated. The ratio mentioned before (a/b) for a rectangle is 1.618.[66] Thus, S_1 and S_2 were calculated by using optimization

techniques. The ratio between S_1 and S_2 is 1.59, which is 98% of the real side ratio for a rectangle (Table 3.3). Hence, the length and width forming the filter area will shape a rectangle form.

Table 3.3. Filter length (S_1), filter width (S_2), and S_1/S_2 ratio.

S_1 (cm)	159
S_2 (cm)	100
A (cm^2)	15900
S_1/S_2	1.59

3.3 Filter Medium

The adsorptive and photocatalytic properties of Mompiche and Quilota iron-titaniferous black sands of Ecuador have been studied by Gomez[13], and the kinetics discoloration of crystal violet is presented in Figure 2.4. shows that Mompiche sand (SEM-205) remove a higher percentage of dye in a shorter period than Quilotoa sand (SXQ-102). Hence, Mompiche sand (SEM-205) is selected as the raw material to develop the adsorptive-photocatalytic process to remove dyes from textile effluents.

The filter medium will be formed by Mompiche sand (SEM-205) of Ecuador and graded gravel (Figure 3.1). The graded gravel will have three layers: The bottom, the middle, and the top layer. The gravel particle diameter varies in each layer, and the porosity and density are considered as constant. The gravel particle size in each layer is stated according to Kawamura[18] design criteria. The particle size of Mompiche sand is reported by Vera[54].
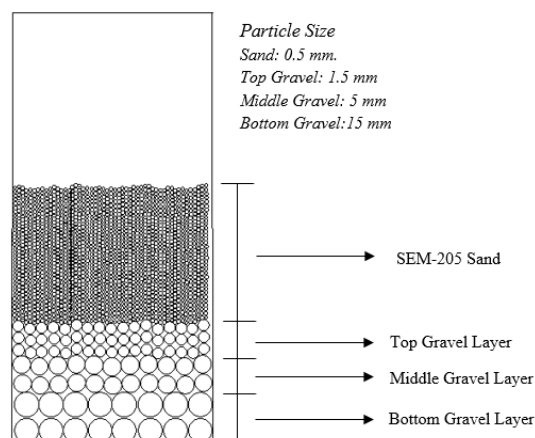
Figure 3.1 Filtration media composed of graded gravel, and iron-titaniferous ecuadorian sand (SEM-205).

3.4 Loss of Pressure (ΔP)

The mean size analysis of several different iron-titaniferous ecuadorian black sands carried out by Vera[54] is shown in Appendix G. Regarding the Mompiche sand (SEM-205), studied by Gomez[13], the mean size reported is 0.54 mm. Thus, the particle diameter of the sand considered for the head loss calculus is 0.5 mm. The density and porosity of Mompiche sand (SEM-205) were obtained by simple experimental design, and the sphericity is stated from literature as a reference value (Table 3.4).

Table 3.4. Sand characteristics to consider in the head loss calculus.

Mean size	0.5 mm
Porosity - e	0.45
Density - ρ	2665.45 kg/m^3
Sphericity - Φ	0.70 [67,68]

The gravel's physical characteristics to be analyzed as the bed support are taken from literature, and they are considered as reference values (Table 3.5).

Table 3.5. Gravel characteristics to consider in the loss of pressure calculus.

Gravel Characteristics	Value	References
Mean size -Bottom Layer	15 mm	[18]
Mean size – Middle Layer	5 mm	[18]
Mean size – Top Layer	1.5 mm	[18]
Porosity - e	0.5	[69]
Density - ρ	2460 kg/m^3	[70]
Sphericity- Φ	0.6	[71]

To calculate the loss of pressure in the filtration medium, equation C.2.13 and C.2.14 are used (See Appendix C). The density and viscosity values of ordinary water will be considered as the density and viscosity of the raw water to be treated (Table 3.6).

Table 3.6. Density and viscosity of water as a function of temperature at atmospheric pressure.[72]

Temperature (°C)	Density (g/mL)	Viscosity (mPa*s)
10	0.99970	1.306
15	0.99910	1.138
20	0.99820	1.002
25	0.99704	0.8901
30	0.99565	0.7974

mPa x s = 10^{-3} Pa x s

The density and viscosity values to be used are at room temperature (20 °C):

$\rho = 998.20$ kg/m^3 (0.99820 g/ml)

$\mu = 1.002 * 10^{-3}$ kg/m*s (1.002 mPa*s)

Each layer forming the granular medium is analyzed (Table 3.7). The proportionality between the sand depth and the gravel depth considered is 2:1.[15,17,18] To determine the loss of pressure, the friction factor needs to be calculated.

Table 3.7. Loss of pressure across the different layer forming the filter medium.

Parameters	Diameter (mm)	Porosity	Height (cm)	Sphericity Φ	Re	Fp	ΔP/m (Pa/m)
Sand	0.5	0.45	30	0.7	0.023	5204.37	192.02
Bottom gravel layer	15	0.5	5	0.6	0.680	185.68	0.177
Middle gravel layer	5	0.5	5	0.6	0.227	553.54	1.58
Upper gravel layer	1.5	0.5	5	0.6	0.068	1841.06	17.51

Then, the total loss of pressure in the filtration medium is determined by the addition of each layer's loss of pressure (Table 3.8).

Table 3.8. Total loss of pressure in the filter design.

Total ΔP (Pa)	58.57
Total $\Delta P/L$ (Pa/m)	211.28

3.5 Fluidization

It is stated that the raw water to be treated in the designed filter must be pre-treated regarding the total suspended solids. Nevertheless, it is known that the suspended solids cannot be removed in 100%. Considering a small number of suspended solids still present in the raw water, these will deposit on the sand grains surface. The deposited solids will disturb the adsorption-photocatalytic process by reducing the contact between the sand grains surface area and the dissolved dye molecules. Thus, one of the primary purposes of fluidization is to remove and drain the deposited solids. To calculate the minimum fluidization velocity to fluidize the sand bed (V_{om}), equation D.1.6 is used (See Appendix D). The minimum fluidization porosity (ε_M) is a given parameter, and it is obtained by quadratic regression

(Figure 3.2) from data taken from the literature as a reference value for further calculations (Table 3.9).

Table 3.9. Particle diameter and void fraction values at incipient fluidization.[67]

Types of particles	Particle size, D_p (mm)			
	0.06	0.10	0.20	0.40
	Void Fraction, (ε_M)			
Sharp Sand ($\Phi = 0.67$)	0.60	0.58	0.53	0.49
Round Sand ($\Phi = 0.86$)	0.53	0.48	0.43	0.42
Anthracite coal ($\Phi = 0.63$)	0.61	0.60	0.56	0.52

As stated before, the reference value for the sand sphericity is 0.70, so the void fraction associated with sharp sand is considered to obtain the reference value for ε_M by a quadratic regression.
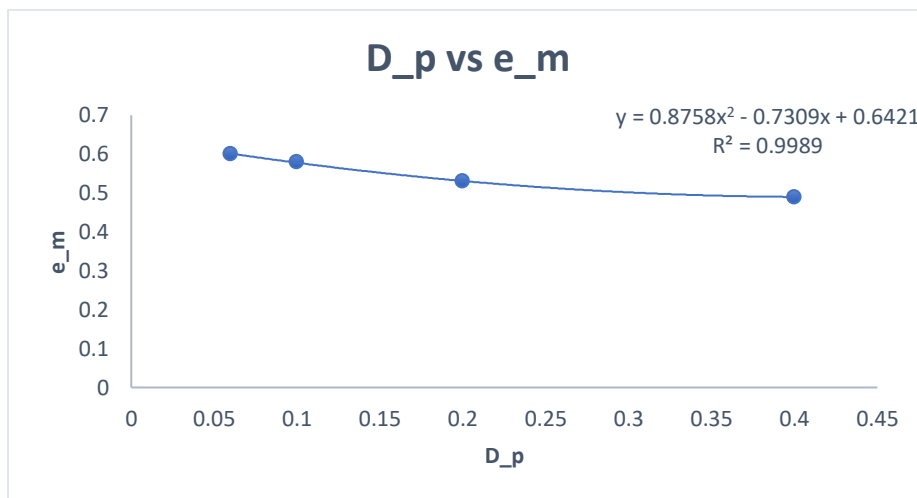
Figure 3.2. Quadratic regression between particle diameter and void fraction at incipient fluidization.

Then, for a particle diameter D_p equal to 0.5 mm. At the minimum fluidization velocity, the porosity ε_M is 0.5.

At incipient fluidization, the minimum fluidization velocity (V_{om}), the height of the bed (L_m), and the bed expansion percentage are determined (Table 3.10).

Table 3.10. Minimum fluidization velocity and void fraction at Incipient Fluidization.

V_{om} (cm/s)	0.32
ε_M (sand)	0.50
ε_1	0.45
L_1 (cm)	30
ε_M	0.50
L_m (cm)	33.3
Expanded bed %	11.0

To backwash the sand bed with the ultimate purpose of removing deposit solids, the sand bed expansion ranges between 15% and 30%.[15] Table 3.11 shows the flow velocity (Vo) required to expand the sand bed in 15% and 30%. Moreover, the porosity (ε) of the expanded bed is calculated using the equation D.2.1 by optimization techniques. The height of the expanded bed (L expanded) is determined by the equation D.2.3 (see Appendix D). As the height of the expanded bed is calculated (L expanded), the space required to perform the bed expansion may also be determined. The free space forming part of the proposed freeboard in the filter is determined by stating the 50% sand bed expansion (Table 3.11). Simply put, the filter will allow a 50% sand bed expansion before sand drainage through the triangular weir.

Table 3.11. Flow velocity, porosity and height of the expanded bed, and space in freeboard required for the bed fluidization.

Bed Expansion	15 %	30 %	50 %
V_o (cm/s)	0.38	0.59	0.9
ε_0	0.45	0.45	0.45
ε	0.52	0.58	0.63
L_0 (cm)	30	30	30
L (cm)	34.3	38.9	44.9
Length expanded (cm)	35	39	45
Space in Freeboard (cm)	5.0	9.0	**15.0**

Furthermore, fluidization will be performed to drain the saturated sand bed mechanically when it lost the adsorptive and photocatalytic properties and must be regenerated or replaced. At flow velocities (V_o) above the minimum fluidization velocity (V_{om}), the fluidized sand will expand and behave like a fluid. Thereby, the sand bed may be drained mechanically through the proposed triangular weir. To remove the sand bed through the triangular weir, the flow velocity must be higher than the flow velocity (V_o) corresponding to the 50% sand bed expansion by fluidization (Table 3.11). Thus, the over 50% expanded san bed will be drained by the triangular weir. Besides, the calculus of the minimum fluidization velocity of the top

gravel layer shows a value of 1.90 cm/s which demonstrates that the flow velocity associated with the sand drainage will not fluidize the gravel support.

3.6 Triangular Weir

A side weir is defined as hydraulic control structure to divert flow into a side channel when the water level exceeds a defined limit. The selection of weir structures depends on the appropriate head-discharge to obtain the required performance in terms of up-stream water level.[73] A triangular weir is designed with the final purpose of draining the up-stream backwash water during backwashing. Furthermore, if the sand has lost its adsorptive and photocatalytic properties, it can be removed through the side weir by solid-water fluidization. The stated V_o (cm/s) is multiplied by the filter area (A) to obtain the flow rate to be drained. It is known that the sand bed expansion during backwash ranges between 15% and 30%. Nevertheless, the filter design in this study considers the bed expansion up to 50%. In this way, the flow rate needed to expand the 50% of the sand bed is considered to calculate the flow rate to be drained during backwashing. However, an overdesign factor of 50% is proposed to calculate the required capacity flow discharging of the weir (Required Q_c) (Table 3.12). Since the discharging flow of the triangular weir is dependent on the height of the weir, the height is defined as 0.2 m. The general formula to calculate the flow discharging of a triangular weir is described by equation E.5 (see Appendix E). Moreover, the effective head (h_e) which includes the variable dependent on the weir angle (k) is calculated (Table 3.12). Thereby, the total capacity of flow discharging (Total Q_c) is higher than the Required Q_c as shown in Table 3.12.

Table 3.12. Required discharging flow capacity for the proposed weir.

Flowrate to drain (l/s)	14.31
Overdesign Factor %	50
Required Q_c (l/s)	21.47
h (cm)	20
k	0.0028
h_e (cm)	20.28
C	0.60
Total Q_c (l/s)	26.0

3.7 Underdrain System

Due to inexpensive cost, simple construction, and the accurate flow distribution, the manifold pipe with perforated laterals is selected as the underdrain system (Figure 3.3). One of the fundamental purposes of the underdrain system is to collect the treated water while the granular filter media remains at rest. Since the particle size of the gravel bottom layer ranges between 15 mm and 25 mm, perforation's diameter in the laterals is 14 mm. This fact lies in the standard hole saw drill bit is 9/16" (14 mm). The irregular shape and the gravel particles size at the bottom layer assure that the filter media is retained. Moreover, PVC is chosen to be the inert raw material for the underdrain construction. Once the filter length and width are established, the perforated laterals and the perforation in the laterals must be equally spaced to warranty the flow uniformity during backwashing (Figure 3.4). Besides, the standard external diameter of the manifold and perforated laterals is 2-1/2" (6.35 cm).
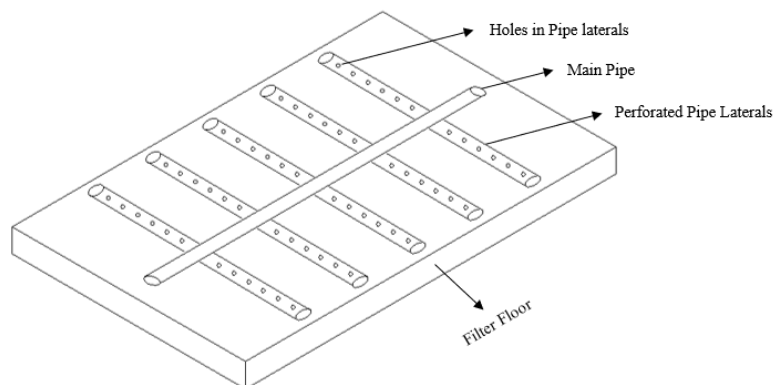
Figure 3.3. Sketch of the main fold with perforated laterals selected as the underdrain system.
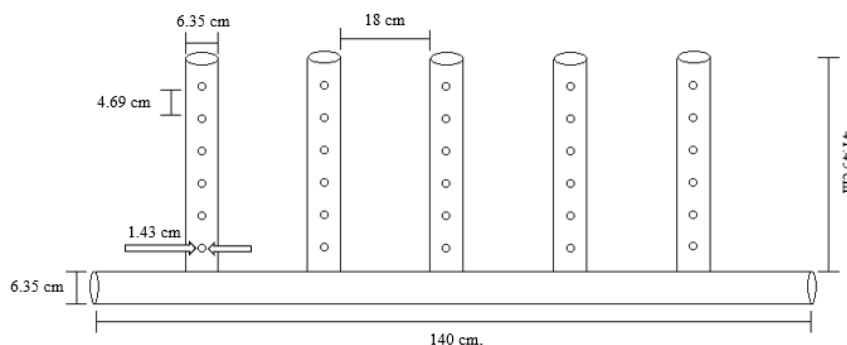
Figure 3.4. Illustration of the sizing in the main fold, perforated lateral, and perforations.

3.8 Filter Depth

The filter design of this study is targeted to dye removal purposes by adsorption and photocatalytic process. Nevertheless, since the sand filters are widely used in wastewater treatment, it would be interesting to achieve the same characteristics of a typical sand filter to stimulate the filter device's acceptance within the textile industry. The proportionality between the sand depth and the gravel depth in a conventional filter is 2:1, as observed in Table 3.13.

Table 3.13. Reference values of general physical dimensions of a conventional slow sand filter.

Parameter	Value (cm)	Reference
Sand layer depth	60	[15,17]
Gravel support layer depth	30	[17,18]

As the sand depth is already determined, the gravel depth is defined using this proportionality. To achieve the characteristics of a conventional sand filter, the following analysis is presented.

The weight percentage of sand in the whole filtration medium is calculated. The density (2665.45 kg/m^3) and porosity (e = 0.45) of Mompiche sand from Ecuador were determined experimentally and are considered for the calculus. Table 3.14 shows the physical dimensions of the filtration medium obtained from the literature and, in a particular case, from the US Patent 4 765 892 by Hulbert[63] regarding a pilot-scale sand filter.

Table 3.14. Physical dimensions of a conventional and a pilot scale sand filter.

	Conventional Sand Filter Values from Literature		Pilot Scale Sand Filter US Patent 4 765 892 by Hulbert[63]	
	Sand	**Gravel**	**Sand**	**Gravel**
Filter Area (m^2)	91.0[11]		3.0	
Height (m)	0.6[15,17]	0.3	0.613	0.305
Weight (kg)	80044	33579	2696	1125
Density (kg/m^3)	2665	2460	2665	2460
Porosity	0.45	0.5	0.45	0.5
Total Weight (kg)	113623		3821	
Wt%	**70.45**	29.55	**70.55**	29.45

It is observed that in a conventional and a particular pilot-scale sand filter, the weight percentage of the sand bed regarding the whole filtration medium is 70%. In view of these facts, the filter design of this study is targeted to have the same sand weight proportion in the filtration medium. Figure 3.5 shows the proposed filter space distribution. The freeboard was determined by the hydraulic profile of the pilot-scale filter and the height for the headwater is explained below.

		(cm)
Filter space	Freeboard	35
	Headwater	25
	Sand Bed	30
	Gravel	15
Underdrain system		

Figure 3.5. Physical space distribution for a sand filter targeted to adsorption and photocatalytic processes.

Since the sand and gravel height for the pilot-scale filter has been stated, the sand weight proportion can be calculated (Table 3.15).

Table 3.15. Sand weight proportion in the proposed filter design.

Sand Weight (kg)	699.28
Gravel Weight (kg)	293.36
Wt Sand %	**70.45**

Thereby, the sand weight proportion shows that the sand and gravel height and the filter's physical features are similar to a conventional sand filter. Besides, one striking characteristic of the pilot-scale filter dimensions is to provide portability to perform demo trials in different textile industries.

The primary purpose of the headwater is to dissipate the energy of the incoming flow rate into the filter, which may erode the sand bed layer. To determine the headwater depth, reference values are considered from the literature regarding a typical sand filter (Table 3.16). It is observed that the headwater is 1.2 times the sand depth.

Table 3.16. Reference depth values of gravel support, sand bed, headwater, and freeboard.

Freeboard	30 cm [62]
Headwater	50 cm [62]
Sand Bed	60 cm [63]
Gravel support	30 cm [63]
	Underdrain system

$$\frac{Sand\ Bed}{Head\ water} = \frac{60\ cm}{50\ cm} = 1.2$$

Thus, the space occupied by the constant headwater will be 1.2 times the stated sand bed depth. In other words, the headwater will be 25 cm depth as shown in Figure 3.5.

The freeboard is obtained by the sum of the free space needed to allow the sand bed expansion and the height of the weir, and it has three purposes:

1) To enable the bed to expand during backwashing.

2) To avoid flooding if the flow rate increases.

3) To contain the weir.

Since the length, width, area, and height of the filter have been stated, Figure 3.6 illustrates the filter box sketch.
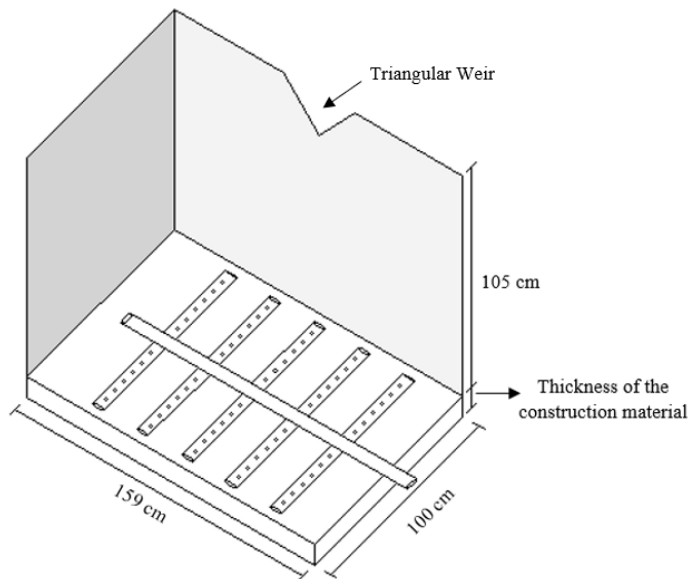
Figure 3.6. Sketch of the filter box and underdrain system.

3.9 Flow Control

As the contact time between the dye molecules and Mompiche sand grains is crucial, the sand bed filter will include two valves: the inlet and outlet valve. Thereby, the raw inlet water, filtration rate, and filter level will be controlled by theses valves when required. Quarter turn valves may be selected to establish and regulate the filtration rate accurately. Figure 3.7 shows the location of the valves and piping.
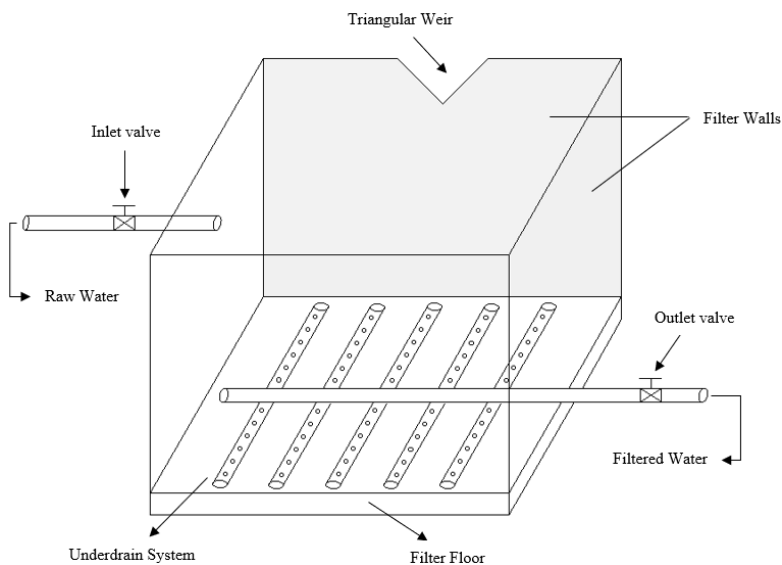
Figure 3.7. Sketch of the filter box that includes the inlet and outlet valve location.

3.10   Pressure on the filter walls

The selection of the raw material to construct the filter depends on the material resistance to fracture, particularly by pressure. In this way, the pressure on the filter walls must be known. To calculate the stress caused by the filtration media and the fluid inside the filter, two scenarios are analyzed: The pressure caused by the solid in the filter and the pressure due to the liquid. These two pressures are calculated separately in horizontal and vertical directions, and the total pressure in the filter will be the sum of each. Values in Table 3.17 are needed.

Table 3.17. Constant of the sand at rest, density, specific weight, and height values of the filtration medium to calculate the pressure exerted in the filter.

γ gravel (kN/m^3)	24.132
γ sand (kN/m^3)	26.148
γ water (kN/m^3)	9.792
k_o sand	0.48
Sand height (cm)	45
Water height (cm)	82.5

Table 3.18 shows the horizontal and vertical pressure in the sand filter. Equation F.1.1 was used to calculate the horizontal pressure exerted by the liquid, and equation F.1.2 for the solid (see equations in Appendix F). Although the solid is formed by the graded gravel and the sand grains, sand only is considered as the solid due to its higher density. It means that the depth of the gravel is considered as sand. The water present in the void fraction of the gravel and sand bed is considered as part of the fluid. Then, the void fraction of the solid volume occupied by water is added to the total height of the water. To determine the overall height occupied by water, the calculus considers the freeboard and the headwater as a full volume of fluid.

Table 3.18. Horizontal and vertical pressure exerted in the filter walls.

Pressure	Vertical Direction	Horizontal Direction
Pressure by sand (kN/m^2)	5.65	11.77
Pressure by sand (psi)	0.82	1.71
Pressure by water (kN/m^2)	3.93	7.86
Pressure by water (psi)	0.57	1.14
Pressure on the walls (kN/m^2)	9.58	19.63
Pressure on the walls (psi)	1.39	2.85

Equation F.2.1 is applied for the vertical pressure due to the liquid and equation F.2.2 for the horizontal stress caused by the solid (See Appendix F).

Since the pressure exerted in the vertical and horizontal direction by the solid and water are known, the thickness of the raw material for the construction of the prototype can be selected compared to the resistance to fracture of a material as provided in its technical specifications sheet.

3.11   Container for sand drainage and backwashing water

The sand must be drained and replaced when its adsorptive and photocatalytic properties have been lost. Since the sand drainage is performed by fluidization, a container is placed on one side of the filter box. This device will receive and drain the backwashing water (Figure 3.8). Moreover, this container may be used as a storage tank to allow the sand grains to sediment for further treatment or final disposal of the sand bed drained.
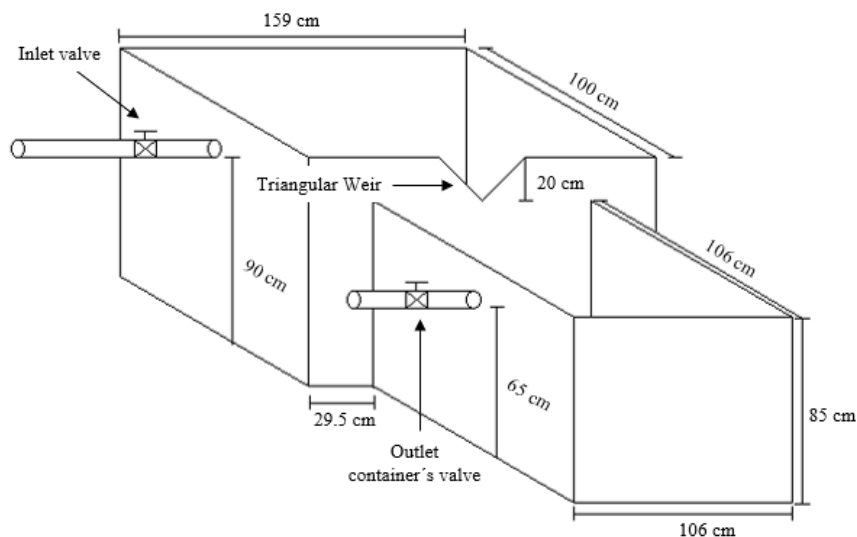
Figure 3.8. Sketch of the filter tank and the container for the sand drainage and backwashing water.

3.12   Selection of raw material for the filter construction

Advanced oxidation processes encompass different methods of oxidant generation and may potentially perform different mechanisms for organic destruction.[74] Gomez[13] reports high decolorization percentage of crystal violet from water in a H_2O_2/UV system using the iron-

titaniferous sands of Ecuador. TiO_2 is a feasible, non-toxic, and chemical stable photocatalyst. When TiO_2 is irradiated with UV generate hydroxide radicals to oxidize organic pollutants. The oxidation process occurs when TiO_2 absorbs a light photon more energetic than its bandgap in the presence of UV light or sunlight.[75] Thus, a UV lamp must be integrated in the construction material of the filter to perform the photocatalytic process. The raw material targeted to contain the filter bed should be chemical stable, malleable, ligh-weight, and low cost. Moreover, the construction material must withstand the pressure exerted by the filter medium and water contained in the filter. Thus, a high-density polymer should be selected. High-density polyethylene would be one of the best raw materials for the pilot-scale filter construction. The thickness of the construction material will be selected by analyzing the tensile and yield strength.

3.13   Recommendation for dye removal effectiveness evaluation

To study the effectiveness of the decolorization process, two methods may be carried out.

1.- A simple and straightforward measuring method using a colorimeter checker. A portable and digital colorimeter checker HI727 provided by HANNA Instruments is considered as the equipment to perform this method (Figure 3.9). This instrument measures the true color of water, and it is used in drinking water and wastewater. The color is measured in Platinum-Cobalt units (Pt-Co or PCU). The technical specifications of the HI727 instrument can be observed in Table 3.19.

Figure 3.9. Illustration of the colorimeter checker (HI727 instrument provided by HANNA Instruments) proposed to evaluate the effectiveness of the filter design.

Table 3.19. Technical specifications of HI727 instrument provided by HANNA Instruments.

Range	0 to 500 PCU
Resolution	5 PCU
Accuracy	$\pm$ 10 PCU $\pm$ 5% of reading @ 25°C / 77°F
Light source	Light Emitting Diode @ 470 nm
Light Detector	Silicon Photocell
Method	Colorimeter method Platinum - Cobalt
Environmental Conditions	0 to 50 °C (32 °F to 122 °F)
Battery	1 x 1.5V AAA
Dimensions	81.5 x 61 x 37.4 mm (3.2 x 2.4 x 1.5")
Weight	64 g (2.25 oz.)

The maximum value measure by HI727 instrument is 500 PCU. Commonly, textile wastewater presents values below 500 PCU, as shown in Table 3.20. However, textile effluents may also present high coloration expressed in high Pt-Co color units, as reported by Syafalni[76], Uysal[77], Lim[78], and Ahmad[79] (Table 3.20).

Table 3.20. Reported textile effluent characteristics from different sources and countries.

Source	Country	Color (Pt-Co)	pH	Reference
Textile effluent for rinsing step of a denim textile industry	Mexico	330	6.84	[80]
Textile effluent from dyeing process	Spain	300	6.9	[81]
Raw Textile water	India	245 - 260	7.8 – 9.0	[82]
Textile wastewater from Al-Hilla factory	Iraq	85	7.9 – 8.5	[83]
Textile wastewater passed from an activated sludge unit	China	310 – 325[a]	8.0 – 8.3	[84]
Dye wastewater sampled from Penfabric Mill	Malaysia	680 – 750	9.0 – 10.18	[76]
Textile wastewater from Al-Khadimia factory	Iraq	50 – 65	7.0 – 9.5	[83]
Wastewater from textile factory located in Busia city	Turkey	1400 - 3000	7.72 – 8.72	[77]
Textile wastewater from a Garment Factory	Malaysia	76-1777.33	3.85 – 11.40	[78]
Textile wastewater after Primary treatment from Kim Fashion Knitwear (M) Sdn. Bhd.	Malaysia	500	8.40	[85]
Effluent after activated sludge treatment from a Cotton Textile Mill.	Malaysia	450 – 650	7.0 – 8.0	[79]

[a] American Dye Manufacturer´s Institute Unit.

If the color measurement is below 500 PCU, the first method may be applied, the measurements can be performed even in situ, and color units vs. time may be plotted for further analysis. Nevertheless, if the color measurement is higher than 500 PCU, the second proposed method must be carried out.

2.- The second method to evaluate the effectiveness of decolorization considers absorbance measurements. Since the wavelength associated with textiles dyes are in the visible-light range, a UV-VIS spectrophotometer is required. Thus, the decolorization effectiveness may be defined as:

$$\frac{Abs_{init} - Abs_{sample}}{Abs_{init}} \; x \; 100 = Color\; Removal \; (\%) \qquad (\;7\;)$$

Then, absorbance values vs. time can be plotted for further analysis.

Chapter IV

Conclusions and Recommendations

4.1 Conclusions

This study has led us to set up the sizing and modular design for a pilot-scale slow sand filter construction that allows the performance of dye removal demo trials in different textile factories. By analyzing the hydraulic performance, simple construction, and promising dye removal rate by the iron-titaniferous ecuadorian sands, this thesis has established a pilot-scale conventional sand filter operation to encourage the adsorption and photocatalytic process acceptance within the textile wastewater treatment.

Interestingly, the design criteria stated and considered in this study enables the implementation of the sand filter to real textile wastewater treatments to handle up to 5% of the textile effluents from the textile industries operated in Tungurahua province. The effectiveness evaluation proposal for the dye removal process results in an attractive, simple, affordable, and accurate method to evaluate the filter performance in the field.

The hydraulic requirements and the dimensions of the underdrain system, filter depth and triangular weir permit to accomplish the filter backwashing and sand bed fluidization by uniformity up-flow water. The filter pressure calculation determines the thickness selection criteria of the raw material for the sand filter construction. Furthermore, the weir and small side tank included in the pilot scale sand filter design allow the sand bed drainage and storage for further treatment, either the regeneration of the usable adsorptive properties or the final disposal.

The dye removal process exploiting the adsorptive and photocatalytic properties of the iron-titaniferous ecuadorian sands was contrasted with the conventional textile decoloring methods. In the first instance, considering the efficiency, economic feasibility, and non-dosage of a chemical or biological compound, the dye removal technology using the

ferruginous sands indicates to be a promising textile effluents treatment method to reduce the environmental impact of its discharging.

Last but not least, based on quantitative and qualitative analysis, it can be inferred that iron-titaniferous ecuadorian sands may be applied in decoloring purposes for textile effluents at the industrial scale.

4.2 Recommendations

(1)   Based on the previous calculations, experimental data of the ecuadorian ferruginous sands, especially from Mompiche sand, is needed. Hence, the minimum fluidization velocity, porosity at incipient fluidization, particle diameter, and sphericity must be determined experimentally.

(2)   To better understand the degradation of the dyes, future studies should address the kinetics of dye removal in the dynamic state using iron-titaniferous sands of Ecuador. Furthermore, the highest decoloring rate in adsorption and photochemical processes may be determined by evaluating enriched sands.

(3)   Further research is needed to perform the adsorption dynamic process to study the effective mass transfer zone and the time saturation of a specific sand bed height. These results may demonstrate the relation between sand height and dye removal efficiency and the useful time before sand bed regeneration.

(4)   The adsorption and photochemical process in this study propose to use the remnant hydrogen peroxide (H_2O_2) from the textile processes for decoloring textile effluents. Additional research is necessary to evaluate and state the best hydrogen peroxide concentration to achieve dye removal process's highest efficiency.

(5)   Ferruginous ecuadorian sand is the raw material of the sand filter designed. The environmental impact analysis of the exploitation of the iron-titaniferous black sands of Ecuador must be studied to set up the vision of this emerging technology.

(6)   Regeneration of the saturated sand bed demands further research in thermal and chemical treatment methods with the ultimate purpose of recovering adsorptive and photocatalytic properties.

(7)   A zeolite layer may be considered as part of the granular media with the essential purpose of generating a rectifying zone where the dyes which are not removed in the sand bed layer may be adsorbed. The assessment of the dye adsorption in zeolites is needed to explore this effect.

(8)   Real textile wastewater encompasses a mixture of different dyes and chemical compounds. This fact may affect the dye removal process rate. Therefore, demo trials using real textile effluents to study and evaluate the dye removal effectiveness of the iron-titaniferous ecuadorian sands is recommended.

(9)   Iron-titaniferous ecuadorian sands must be replaced when it has lost the adsorptive and photocatalytic properties. The final disposal of the saturated and non-regenerable sand by-product must be addressed. At first instance, further analysis in the application as raw material for brick construction is recommended.

(10)   The suggested colorimeter HI727 instrument does not measure color units above 500 PCU. On this basis, a standardized dilution protocol profile correlation should be established with the ultimate purpose of determining color units above 500 PCU is recommended.

Bibliography

(1)   Verma, A. K.; Dash, R. R.; Bhunia, P. A Review on Chemical Coagulation/Flocculation Technologies for Removal of Colour from Textile Wastewaters. *J. Environ. Manage.* **2012**, *93* (1), 154–168. https://doi.org/10.1016/j.jenvman.2011.09.012.

(2)   Asociación de Industriales Textiles del Ecuador (AITE). Industria Textil y Confección: El Reto de Subsistir. Boletín Mensual AITE 2016, p 6.

(3)   Wang, Y.; Gao, B. Y.; Yue, Q. Y.; Wei, J. C.; Zhou, W. Z.; Gu, R. Color Removal from Textile Industry Wastewater Using Composite Flocculants. *Environ. Technol.* **2007**, *28* (6), 629–637. https://doi.org/10.1080/09593332808618824.

(4)   Kant, R. Textile Dyeing Industry an Environmental Hazard. *Nat. Sci.* **2012**, *04* (01), 22–26. https://doi.org/10.4236/ns.2012.41004.

(5)   Joo, D. J.; Shin, W. S.; Choi, J. H.; Choi, S. J.; Kim, M. C.; Han, M. H.; Ha, T. W.; Kim, Y. H. Decolorization of Reactive Dyes Using Inorganic Coagulants and Synthetic Polymer. *Dye. Pigment.* **2007**, *73* (1), 59–64. https://doi.org/10.1016/j.dyepig.2005.10.011.

(6)   Hassan, M. A. A.; Li, T. P.; Noor, Z. Z. Coagulation and Flocculation Treatment of Wastewater in Textile Industry Using Chitosan. *J. Chem. Nat. Resour. Eng.* **2009**, *4* (1), 43–53.

(7)   Drumon, F. M.; Rodrigues de Oliveira, G. A.; Anastácio, E. R.; Cardoso, J. C.; Valnice Boldrin, M.; Danielle Palma de Oliveira. Textile Dyes: Dyeing Process and Environmental Impact. *Eco-Friendly Text. Dye. Finish.* **2013**, *6* (1), 151–176.

(8)   Choi, J. H.; Shin, W. S.; Lee, S. H.; Joo, D. J.; Lee, J. D.; Choi, S. J.; Park, L. S. Application of Synthetic Polyamine Flocculants for Dye Wastewater Treatment. *Sep. Sci. Technol.* **2007**, *36* (13), 2945–2958. https://doi.org/10.1081/SS-100107638.

(9)   Santhy, K.; Selvapathy, P. Removal of Reactive Dyes from Wastewater by Adsorption

on Coir Pith Activated Carbon. *Bioresour. Technol.* **2006**, *97* (11), 1329–1336. https://doi.org/10.1016/j.biortech.2005.05.016.

(10)   Nalco Chemical Company; Kemmer, F. N.; McCallion, J. *The NALCO Water Handbook*; Flynn, D. J., Ed.; McGraw-Hill, 2009.

(11)   Crittenden, J. C.; Trussell, R. R.; Hand, D. W.; Howe, K. J.; Tchobanoglous, G. *MWH's Water Treatment: Principles and Design*; Wiley, 2012. https://doi.org/10.1002/9781118131473.

(12)   Cheremisinoff, N. P.; Knovel (Firm). *Handbook of Water and Wastewater Treatment Technologies*; Chemical, Petrochemical & Process; Elsevier Science, 2002.

(13)   Gomez, J. M. Removal of Crystal Violet Dye from Aqueos Solution Using Ecuadorian Black Sands as Photocatalytic Adsorbents, Undergraduate Thesis. Yachay Tech University, 2020.

(14)   Narendra G, A. S. Accelerated Bleaching of Cotton Material with Hydrogen Peroxide. *J. Text. Sci. Eng.* **2013**, *03* (04). https://doi.org/10.4172/2165-8064.1000140.

(15)   American Water Works Association; Edzwald, J. K. *Water Quality & Treatment: A Handbook on Drinking Water*; Water Resources and Environmental Engineering Series; McGraw-Hill Education, 2010.

(16)   Singh, K. P.; Mohan, D.; Sinha, S.; Tondon, G. S.; Gosh, D. Color Removal from Wastewater Using Low-Cost Activated Carbon Derived from Agricultural Waste Material. *Ind. Eng. Chem. Res.* **2003**, *42* (9), 1965–1976. https://doi.org/10.1021/ie020800d.

(17)   Mackenzie, D. *Water and Wastewater Engineering*; McGraw-Hill, 2017.

(18)   Kawamura, S. *Integrated Design and Operation of Water Treatment Facilities*; Wiley, 2000.

(19)   Soledispa, B.; Villacres, J. Estudio Composicional de Las Arenas Ferrotitaníferas Del Sector Comprendido Entre El Estero Data de Posorja y El Monasterio de Santa Teresa,

Provincia Del Guayas, Ecuador. *Acta Ocean. Pac.* **1990**, *6* (1).

(20)   Babu, N.; Vasumathi, N.; Rao, R. B. Recovery of Ilmenite and Other Heavy Minerals from Teri Sands (Red Sands) of Tamil Nadu, India. *J. Miner. Mater. Charact. Eng.* **2009**, *08* (02), 149–159. https://doi.org/10.4236/jmmce.2009.82013.

(21)   Chuquirima, M.; Cortez, L. Estudio y Obtención de Metal de Hierro a Partir de Arenas Ferruginosas. Tesis de Pregrado, Escuela Politécnica Nacional, 2014.

(22)   Trujillo, D. Desarrollo de Un Proceso de Recuperación de Dióxido de Titanio a Partir de Ilmenita Presente En Las Arenas Ferrotitaníferas de La Zona de Mompinche. Tesis de Pregrado, Escuela Politécnica Nacional, 2015.

(23)   Loaiza, D. Obtención de Dióxido de Titanio (TiO2), a Partir de Ilmenita (FeTiO3), Presente En Arenas Ferrotitaníferas Provenientes Del Sector Congüime, Cantón Paquisha, Provincia de Zamora Chinchipe. Tesis de Pregrado, Universidad Técnica Particular de Loja, 2017. https://doi.org/10.1007/s00281-012-0343-7.

(24)   Zamora, L. I. Caracterización Geológica-Mineragráfica de Las Arenas Ferro-Titaníferas (Fe-Ti) y de Sus Fuentes de Aporte En El Sector de Las Peñas Hasta Playa de Molina (Cantón Eloy Alfaro - Provincia de Esmeraldas). Tesis de Pregrado, Universidad de Guayaquil, 2018.

(25)   Ramalho, R. S.; Beltrán, D. J.; de Lora, F. *Tratamiento de Aguas Residuales*; Reverte, Ed.; REVERTE: Quebec, 1996.

(26)   American Public Health Association; American Water Works Association; Water Environment Federation; Eaton, A. D.; Clesceri, L. S.; Franson, M. A. H.; Rice, E. W.; Greenberg, A. E. *Standard Methods for the Examination of Water & Wastewater*, 21st Editi.; H. Franson, M. A., Ed.; Standard Methods for the Examination of Water and Wastewater; American Public Health Association: Washington, 2005.

(27)   American Water Works Association. *Water Quality*, Third Edit.; American Water Works Association, Ed.; Principles and practices of water supply operations series; American Water Works Association, 2003.

(28)   Pang, Y. L.; Abdullah, A. Z. Current Status of Textile Industry Wastewater Management and Research Progress in Malaysia: A Review. *Clean - Soil, Air, Water* **2013**, *41* (8), 751–764. https://doi.org/10.1002/clen.201000318.

(29)   Clark, M. *Handbook of Textile and Industrial Dyeing: Principles, Processes and Types of Dyes*; Woodhead Publishing, 2011.

(30)   Hao, O. J.; Kim, H.; Chiang, P. C. Decolorization of Wastewater. *Crit. Rev. Environ. Sci. Technol.* **1999**, *30* (4), 449–505. https://doi.org/10.1080/10643380091184237.

(31)   Firmino, P. I. M.; Da Silva, M. E. R.; Cervantes, F. J.; Santos, A. B. dos. Colour Removal of Dyes from Synthetic and Real Textile Wastewaters in One- and Two-Stage Anaerobic Systems. *Bioresour. Technol.* **2010**, *101* (20), 7773–7779. https://doi.org/https://doi.org/10.1016/j.biortech.2010.05.050.

(32)   Stanescu, I.; Manea, L. R.; Bertea, A.; Bertea, A. P.; Sandu, I. C. A. Application of the Taguchi Method in the Optimization of the Photo-Fenton Discoloration of Wastewater from Reactive Blue 19 Dyeing. *Rev. Chim.* **2016**, *67* (10), 2082–2086.

(33)   Prado, A. G. S.; Torres, J. D.; Faria, E. A.; Dias, S. C. L. Comparative Adsorption Studies of Indigo Carmine Dye on Chitin and Chitosan. *J. Colloid Interface Sci.* **2004**, *277* (1), 43–47. https://doi.org/https://doi.org/10.1016/j.jcis.2004.04.056.

(34)   Fazal, S.; Zhang, B.; Zhong, Z.; Gao, L.; Chen, X. Industrial Wastewater Treatment by Using MBR (Membrane Bioreactor) Review Study. *J. Environ. Prot. (Irvine,. Calif).* **2015**, *06* (06), 584–598. https://doi.org/10.4236/jep.2015.66053.

(35)   Robinson, T.; McMullan, G.; Marchant, R.; Nigam, P. Remediation of Dyes in Textile Effluent: A Critical Review on Current Treatment Technologies with a Proposed Alternative. *Bioresour. Technol.* **2001**, *77* (3), 247–255. https://doi.org/https://doi.org/10.1016/S0960-8524(00)00080-8.

(36)   Hai, F. I.; Yamamoto, K.; Fukushi, K. Hybrid Treatment Systems for Dye Wastewater. *Crit. Rev. Environ. Sci. Technol.* **2007**, *37* (4), 315–377. https://doi.org/10.1080/10643380601174723.

(37) Konstantinou, I. K.; Albanis, T. A. TiO2-Assisted Photocatalytic Degradation of Azo Dyes in Aqueous Solution: Kinetic and Mechanistic Investigations: A Review. *Appl. Catal. B Environ.* **2004**, *49* (1), 1–14. https://doi.org/10.1016/j.apcatb.2003.11.010.

(38) Marcucci, M.; Nosenzo, G.; Capannelli, G.; Ciabatti, I.; Corrieri, D.; Ciardelli, G. Treatment and Reuse of Textile Effluents Based on New Ultrafiltration and Other Membrane Technologies. *Desalination* **2001**, *138* (1–3), 75–82. https://doi.org/10.1016/S0011-9164(01)00247-8.

(39) Chen, X.; Shen, Z.; Zhu, X.; Fan, Y.; Wang, W. Advanced Treatment of Textile Wastewater for Reuse Using Electrochemical Oxidation and Membrane Filtration. *Water SA* **2005**, *31* (1), 127–132. https://doi.org/10.4314/wsa.v31i1.5129.

(40) Merzouk, B.; Madani, K.; Sekki, A. Using Electrocoagulation-Electroflotation Technology to Treat Synthetic Solution and Textile Wastewater, Two Case Studies. *Desalination* **2010**, *250* (2), 573–577. https://doi.org/10.1016/j.desal.2009.09.026.

(41) Togo, C. A.; Mutambanengwe, C. C. Z.; Whiteley, C. G. Decolourisation and Degradation of Textile Dyes Using a Sulphate Reducing Bacteria (SRB) - Biodigester Microflora Co-Culture. *African J. Biotechnol.* **2008**, *7* (2), 114–121. https://doi.org/10.5897/AJB08.727.

(42) Meriç, S.; Kaptan, D.; Ölmez, T. Color and COD Removal from Wastewater Containing Reactive Black 5 Using Fenton's Oxidation Process. *Chemosphere* **2004**, *54* (3), 435–441. https://doi.org/10.1016/j.chemosphere.2003.08.010.

(43) Douglas Graham, N. J.; Jiang, J. Preparation and Uses of Polyferric Sulphate. 5,785,862, 1998.

(44) Allen, S. J.; McKay, G.; Khader, K. Y. H. Multi-Component Sorption Isotherms of Basic Dyes onto Peat. *Environ. Pollut.* **1988**, *52* (1), 39–53. https://doi.org/10.1016/0269-7491(88)90106-6.

(45) McKay, G.; Allen, S. J.; McConvey, I. F.; Otterburn, M. S. Transport Processes in the Sorption of Colored Ions by Peat Particles. *J. Colloid Interface Sci.* **1981**, *80* (2), 323–

339. https://doi.org/10.1016/0021-9797(81)90192-2.

(46)   Al Duri, B., McKay, G., El Geundi, M.S., Wahab Abdu, M. . Three Resistance Transport Model for Dye Adsorption onto Bagasse Pitch. *J. Environ. Eng.* **1990**, *116* (3), 487–502.

(47)   McKay, G.; Otterburn, M. S.; Aga, J. A. Fuller's Earth and Fired Clay as Adsorbents for Dyestuffs. *Water. Air. Soil Pollut.* **1985**, *24* (3), 307–322. https://doi.org/10.1007/BF00161790.

(48)   Allen, S. J.; McKay, G.; Khader, K. Y. H. Equilibrium Adsorption Isotherms for Basic Dyes onto Lignite. *J. Chem. Technol. Biotechnol.* **2007**, *45* (4), 291–302. https://doi.org/10.1002/jctb.280450406.

(49)   Mittal, A. K., Venkobachar, C. Sorption and Desorption of Dyes by Sulfonated Coal. *J. Environ. Eng.* **1993**, *119* (2), 366–368.

(50)   Chu, W. Dye Removal from Textile Dye Wastewater Using Recycled Alum Sludge. *Water Res.* **2001**, *35* (13), 3147–3152. https://doi.org/https://doi.org/10.1016/S0043-1354(01)00015-X.

(51)   Gupta, V.; Mohan, D.; Sharma, S.; Sharma, M. Removal of Basic Dyes (Rhodamine B and Methylene Blue) from Aqueous Solutions Using Bagasse Fly Ash. *Sep. Sci. Technol.* **2000**, *35* (13), 2097–2113. https://doi.org/10.1081/SS-100102091.

(52)   Doğan, M.; Alkan, M.; Onganer, Y. Adsorption of Methylene Blue from Aqueous Solution onto Perlite. *Water. Air. Soil Pollut.* **2000**, *120* (3), 229–248. https://doi.org/10.1023/A:1005297724304.

(53)   Ahmed, M. N.; Ram, R. N. Removal of Basic Dye from Waste-Water Using Silica as Adsorbent. *Environ. Pollut.* **1992**, *77* (1), 79–86. https://doi.org/https://doi.org/10.1016/0269-7491(92)90161-3.

(54)   Vera, D. C. Characterization of Ecuadorian Ferruginous and Titaniferous Sands for Hydrogen Sulfide Capture. Undergraduate Thesis, Yachay Tech University, 2020.

(55)   Kucharavy, D.; De Guio, R. Application of S-Shaped Curves. *Procedia Eng.* **2011**, *9*, 559–572. https://doi.org/10.1016/j.proeng.2011.03.142.

(56)   Nieto, M.; Lopéz, F.; Cruz, F. Performance Analysis of Technology Using the S Curve Model: The Case of Digital Signal Processing (DSP) Technologies. *Technovation* **1998**, *18* (6–7), 439–457. https://doi.org/10.1016/S0166-4972(98)00021-2.

(57)   Wong, C. Y.; Chandran, V. G. R.; Ng, B. K. Technology Diffusion in the Telecommunications Services Industry of Malaysia. *Inf. Technol. Dev.* **2014**, *22* (4), 562–583. https://doi.org/10.1080/02681102.2014.949611.

(58)   Sincero, A. P.; Sincero, G. A. *Physical-Chemical Treatment of Water and Wastewater*; CRC Press, 2002.

(59)   Stevenson, D. *Water Treatment Unit Processes*; World Scientific Publishing Company, 1997.

(60)   Lin, S. D.; Lee, C. *Water and Wastewater Calculations Manual, 2nd Ed.*; McGraw Hill professional; McGraw-Hill Education, 2007.

(61)   Visscher, J. T. Slow Sand Filtration : Design, Operation, and Maintenance. *J. - Am. Water Work. Assoc.* **1990**, *82* (C), 67–71. https://doi.org/10.1002/j.1551-8833.1990.tb06979.x.

(62)   Barrett, J. M.; Bryck, J.; Collins, M. R.; Janonis, B. A.; Logsdon, G. S. *Manual of Design for Slow Sand Filtration*; Hendricks, D., Ed.; The Foundation, 1991.

(63)   Hulbert, M.; Currier, J. W. Sand Filter Media and an Improved Method of Purifying Water. 4,765,892, 1988.

(64)   Instituto Nacional de Estadísticas y Censos (INEC). Infoeconomía. Quito-Ecuador 2012.

(65)   Raykov, T.; Marcoulides, G. A. *Basic Statistics: An Introduction with R*; Rowman & Littlefield Publishers, Inc.: Plymouth, 2013; Vol. 50. https://doi.org/10.5860/choice.50-5050.

(66)   Johnson, D. B.; Mowry, T. A. *Mathematics: A Practical Odyssey*, 8th Ed.; Cengage Learning: Boston, 2015.

(67)   Geankoplis, C. J. *Transport Processes and Unit Operations*, 3th ed.; Prentice-Hall International, Inc.: New Jersey, 1993. https://doi.org/10.1016/0300-9467(80)85013-1.

(68)   Summerfelt, S. T. Design and Management of Conventional Fluidized-Sand Biofilters.   *Aquac.   Eng.*   **2006**,   *34*   (3),   275–302. https://doi.org/10.1016/j.aquaeng.2005.08.010.

(69)   Prochaska, C. A.; Zouboulis, A. I. Performance of Intermittently Operated Sand Filters : A Comparable Study, Treating Wastewaters of Different Origins. *Water Air Soil Pollut.* **2003**, *147* (1), 367–388. https://doi.org/10.1023/A:1024550000904.

(70)   Detert, M.; Weitbrecht, V.; Jirka, G. H. Laboratory Measurements on Turbulent Pressure Fluctuations in and above Gravel Beds. *J. Hydraul. Eng.* **2010**, *136* (10), 779–789. https://doi.org/10.1061/(ASCE)HY.1943-7900.0000251.

(71)   Adiotomre, E. E.; Adaikpoh, E. O.; Erhisere, O. The Gravel Packing Chacteristics of Ethiope River Sediments, Southern Nigeria. *World Appl. Sci. J.* **2013**, *24* (6), 759–764. https://doi.org/10.5829/idosi.wasj.2013.24.06.1178.

(72)   Schuck, P.; Zhao, H.; Brautigam, C. A.; Ghirlando, R. *Basic Principles of Analytical Ultracentrifugation*; CRC Press: Florida, 2016. https://doi.org/10.1201/b19028.

(73)   May, R. W. P.; Bromwich, B. C.; Gasowski, Y.; Rickard, C. E. *Hydraulic Design of Side Weirs*; Thomas Telford: Cambridge, 2003. https://doi.org/10.1680/hdosw.31678.

(74)   Miklos, D. B.; Remy, C.; Jekel, M.; Linden, K. G.; Drewes, J. E.; Hübner, U. Evaluation of Advanced Oxidation Processes for Water and Wastewater Treatment – A   Critical   Review.   *Water   Res.*   **2018**,   *139*,   118–131. https://doi.org/10.1016/j.watres.2018.03.042.

(75)   Sridewi, N.; Tan, L. T.; Sudesh, K. Solar Photocatalytic Decolorization and Detoxification of Industrial Batik Dye Wastewater Using P(3HB)-TiO2

Nanocomposite Films. *Clean - Soil, Air, Water* **2011**, *39* (3), 265–273. https://doi.org/10.1002/clen.201000344.

(76)   Syafalni, S.; Abustan, I.; Dahlan, I.; Wah, C. K.; Umar, G. Treatment of Dye Wastewater Using Granular Activated Carbon and Zeolite Filter. *Mod. Appl. Sci.* **2012**, *6* (2), 37–51. https://doi.org/10.5539/mas.v6n2p37.

(77)   Uysal, Y.; Aktas, D.; Caglar, Y. Determination of Color Removal Efficiency of Lemna Minor L. from Industrial Effluents. *J. Environ. Prot. Ecol.* **2014**, *1726* (4), 1718–1726.

(78)   Lim, S. L.; Chu, W. L.; Phang, S. M. Use of Chlorella Vulgaris for Bioremediation of Textile Wastewater. *Bioresour. Technol.* **2010**, *101* (19), 7314–7322. https://doi.org/10.1016/j.biortech.2010.04.092.

(79)   Ahmad, A. A.; Hameed, B. H. Reduction of COD and Color of Dyeing Effluent from a Cotton Textile Mill by Adsorption onto Bamboo-Based Activated Carbon. *J. Hazard. Mater.* **2009**, *172* (2–3), 1538–1543. https://doi.org/10.1016/j.jhazmat.2009.08.025.

(80)   Almazán-Sánchez, P. T.; Linares-Hernández, I.; Solache-Río, M. J.; Martínez-Miranda, V. Textile Wastewater Treatment Using Iron-Modified Clay and Copper-Modified Carbon in Batch and Column Systems. *Water. Air. Soil Pollut.* **2016**, *227* (4). https://doi.org/10.1007/s11270-016-2801-7.

(81)   Buscio, V.; Marín, M. J.; Crespi, M.; Gutiérrez-Bouzán, C. Reuse of Textile Wastewater after Homogenization-Decantation Treatment Coupled to PVDF Ultrafiltration Membranes. *Chem. Eng. J.* **2015**, *265* (1), 122–128. https://doi.org/10.1016/j.cej.2014.12.057.

(82)   Manekar, P.; Patkar, G.; Aswale, P.; Mahure, M.; Nandy, T. Detoxifying of High Strength Textile Effluent through Chemical and Bio-Oxidation Processes. *Bioresour. Technol.* **2014**, *157*, 44–51. https://doi.org/10.1016/j.biortech.2014.01.046.

(83)   Al-Shuwaiki, N. M.; Abid, B. A.; Brbooti, M. M. Color Removal from Industrial Textile Wastewater Using Chemical Adsorption. *Eng. Technol. J.* **2013**, *31* (4), 471–

489.

(84)   Qian, F.; Sun, X.; Liu, Y. Removal Characteristics of Organics in Bio-Treated Textile Wastewater Reclamation by a Stepwise Coagulation and Intermediate GAC/O3 Oxidation Process. *Chem. Eng. J.* **2013**, *214*, 112–118. https://doi.org/10.1016/j.cej.2012.09.130.

(85)   Chu, W. L.; See, Y. C.; Phang, S. M. Use of Immobilised Chlorella Vulgaris for the Removal of Colour from Textile Dyes. *J. Appl. Phycol.* **2009**, *21* (6), 641–648. https://doi.org/10.1007/s10811-008-9396-3.

(86)   Couper, J. R.; Penney, W. R.; Fair, J. R.; Walas, S. M. *Chemical Process Equipment: Selection and Design*, 2nd. ed.; Elsevier Science: Massachusetts, 2005.

(87)   McCabe, W. L.; Smith, J. C.; Harriott, P. *Unit Operations of Chemical Engineering*, 5th ed.; Clark, B. J., Castellano, E., Eds.; McGraw-Hill: Singapore, 1993.

(88)   Ortega-Rivas, E. *Unit Operations of Particulate Solids Theory and Practice*; CRC Press, 2012. https://doi.org/10.1016/S0065-2113(08)60505-2.

(89)   Siwiec, T. The Sphericity of Grains of Filtration Beds Applied for Water Treatment on Examples of Selected Minerals. *Electron. J. Polish Agric. Univ. Ser. Civ. Eng.* **2007**, *10*.

(90)   Brown, G. G.; Foust, A. S.; Katz, R. L.; Schneldewind, R.; Wood, W. P.; Brown, G. M. Unit Operations. CBS Publishers & Distributors: New Delhi 1950.

(91)   Ghodsian, M. Flow over Triangular Side Weir. *Sci. Iran.* **2004**, *11* (1–2), 114–120.

(92)   Chanson, H.; Wang, H. Unsteady Discharge Calibration of a Large V-Notch Weir. *Flow Meas. Instrum.* **2013**, *29*, 19–24. https://doi.org/10.1016/j.flowmeasinst.2012.10.010.

(93)   Reddy, M. S.; Reddy, Y. R. Experimental Investigation on the Influence of Density of Fluid on Efficiency of V- Notch. *Int. J. Adv. Sci. Res. Eng.* **2017**, *3* (9), 35–41. https://doi.org/10.7324/ijasre.2017.32515.

(94)   Shen, J. *Discharge Characteristics of Triangular-Notch Thin-Plate Weirs*; Interior, U. S. D. of the, Ed.; Discharge Characteristics of Triangular-notch Thin-plate Weirs; United States Department of the Interior, Geological Survey: Washington, 1981.

(95)   Gerhart, P. M.; Gerhart, A. L.; Hochstein, J. I. *Fundamentals of Fluid Mechanics*, 8th Ed.; Ratts, L., Ed.; Don Fowley, 2016.

(96)   Purushothama, P. *Soil Mechanics and Foundation Engineering*, 2nd. Ed.; PEARSON, 2013.

(97)   Hall, A. S.; Archer, F. E.; Gilbert, R. I. *Engineering Statics*, 2nd Ed.; University of New South Wales Press Ltd: Hong Kong, 1999.

(98)   Ishibashi, I.; Hazarika, H. *Soil Mechanics Fundamentals and Applications*, 2nd ed.; CRC Press: Boca Raton, 2015. https://doi.org/10.1201/b16655.

(99)   Bodó, B.; Jones, C. *Introduction to Soil Mechanics*; Wiley: Oxford, 2013.

Appendices

Appendix A: Discharging Flows of Factories of Fabrics and Textile Finishing located in Tungurahua.

Table A.1 Maximum and minimum reported discharging flows of factories of fabrics and textile finishing operated in Tungurahua province.

CATEGORIZATION	LOCATION	Q (l/s)	pH
FACTORY OF FABRICS AND TEXTILE FINISHING	PELILEO	3,21	6,45
		0,15	5,17
FACTORY OF FABRICS AND TEXTILE FINISHING	PELILEO	1,47	6,29
		0,79	7,28
FACTORY OF FABRICS AND TEXTILE FINISHING	PELILEO	2,45	7,03
		1,21	6,48
FACTORY OF FABRICS AND TEXTILE FINISHING	PELILEO	0,95	7,43
		0,93	6,31
FACTORY OF FABRICS AND TEXTILE FINISHING	PELILEO	3,04	6,09
FACTORY OF FABRICS AND TEXTILE FINISHING	PELILEO	2,47	4,41
		0,81	4,31
FACTORY OF FABRICS AND TEXTILE FINISHING	PELILEO	2,24	5,3
FACTORY OF FABRICS AND TEXTILE FINISHING	PELILEO	N-R	7,52
		0,87	8,16
FACTORY OF FABRICS AND TEXTILE FINISHING	PELILEO	4,2	8,11
		1,51	6,93
FACTORY OF FABRICS AND TEXTILE FINISHING	PELILEO	2	8,19
FACTORY OF FABRICS AND TEXTILE FINISHING	PELILEO	0,24	6,26
FACTORY OF FABRICS AND TEXTILE FINISHING	PELILEO	1,87	7,18
		N-R	7,12
FACTORY OF FABRICS AND TEXTILE FINISHING	PELILEO	3,22	6,11
		0,78	8,22
FACTORY OF FABRICS AND TEXTILE FINISHING	PELILEO	N-R	<4
		1	4,74
FACTORY OF FABRICS AND TEXTILE FINISHING	PELILEO	3,63	5,34
FACTORY OF FABRICS AND TEXTILE FINISHING	PELILEO	1,25	6,91
		0,25	6,22
FACTORY OF FABRICS AND TEXTILE FINISHING	PELILEO	0,77	7,37
		0,84	7,14
FACTORY OF FABRICS AND TEXTILE FINISHING	PELILEO	1,72	4,95
		0,22	6,47
FACTORY OF FABRICS AND TEXTILE FINISHING	PELILEO	1,68	6,18
		1,2	7,34
FACTORY OF FABRICS AND TEXTILE FINISHING	PELILEO	0,73	6,67
FACTORY OF FABRICS AND TEXTILE FINISHING	PELILEO	0,12	6,74
FACTORY OF FABRICS AND TEXTILE FINISHING	PELILEO	0,98	7,06
		0,40	7,19

FACTORY OF FABRICS AND TEXTILE FINISHING	PELILEO	2,03	6,87
		0,14	8,56
FACTORY OF FABRICS AND TEXTILE FINISHING	PELILEO	2,16	6,76
FACTORY OF FABRICS AND TEXTILE FINISHING	PELILEO	0,73	6,25
		1,8	8,08
FACTORY OF FABRICS AND TEXTILE FINISHING	PELILEO	0,44	6,97
		0,79	7,19
FACTORY OF FABRICS AND TEXTILE FINISHING	PELILEO	1,9	6,46
		0,57	7,5
FACTORY OF FABRICS AND TEXTILE FINISHING	PELILEO	8,88	6,9
		0,67	7,12
FACTORY OF FABRICS AND TEXTILE FINISHING	PELILEO	0,44	6,65
		N-R	
FACTORY OF FABRICS AND TEXTILE FINISHING	PELILEO	N-R	6,52
		2,43	5,93
FACTORY OF FABRICS AND TEXTILE FINISHING	PELILEO	1,9	6,18
FACTORY OF FABRICS AND TEXTILE FINISHING	PELILEO	0,72	6,22
		0,81	7,29
FACTORY OF FABRICS AND TEXTILE FINISHING	PELILEO	N-R	7,19
		0,15	7,16
FACTORY OF FABRICS AND TEXTILE FINISHING	PELILEO	N-R	N-R
FACTORY OF FABRICS AND TEXTILE FINISHING	PELILEO	0,56	6,53
FACTORY OF FABRICS AND TEXTILE FINISHING	PELILEO	2,41	6,73
		0,97	7,23
FACTORY OF FABRICS AND TEXTILE FINISHING	PELILEO	1,2	6,71
		0,17	6,6
FACTORY OF FABRICS AND TEXTILE FINISHING	PELILEO	3,3	7,16
FACTORY OF FABRICS AND TEXTILE FINISHING	PELILEO	N-R	N-R
FACTORY OF FABRICS AND TEXTILE FINISHING	PELILEO	0,64	6,21
		1,04	7,11
FACTORY OF FABRICS AND TEXTILE FINISHING	PELILEO	N-R	6,69
FACTORY OF FABRICS AND TEXTILE FINISHING	PELILEO	N-R	7,19
		1,47	6,08
FACTORY OF FABRICS AND TEXTILE FINISHING	PELILEO	1,2	6,42
		0,88	6,36
FACTORY OF FABRICS AND TEXTILE FINISHING	PELILEO	0,68	7,05
		0,14	7,35
FACTORY OF FABRICS AND TEXTILE FINISHING	PELILEO	2,12	7,41
FACTORY OF FABRICS AND TEXTILE FINISHING	AMBATO	0,39	6,96
		0,74	7,16
FACTORY OF FABRICS AND TEXTILE FINISHING	AMBATO	1,2	8,8
		1,52	7,82
FACTORY OF FABRICS AND TEXTILE FINISHING	AMBATO	N-R	N-R
FACTORY OF FABRICS AND TEXTILE FINISHING	AMBATO	2,03	7,49
FACTORY OF FABRICS AND TEXTILE FINISHING	AMBATO	2,72	5
		2,56	5,02
FACTORY OF FABRICS AND TEXTILE FINISHING	AMBATO	N-R	N-R
FACTORY OF FABRICS AND TEXTILE FINISHING	AMBATO	1	6,65
FACTORY OF FABRICS AND TEXTILE FINISHING	AMBATO	1,96	6,32
		5	6,57

FACTORY OF FABRICS AND TEXTILE FINISHING	AMBATO	5,61	6,93
		1,96	6,7
FACTORY OF FABRICS AND TEXTILE FINISHING	AMBATO	2,75	7,65
		1,2	N-R
FACTORY OF FABRICS AND TEXTILE FINISHING	AMBATO	1,72	6,85
		0,1	6,94
FACTORY OF FABRICS AND TEXTILE FINISHING	AMBATO	0,75	6,98
		0,12	9,79
FACTORY OF FABRICS AND TEXTILE FINISHING	AMBATO	2,04	7,15
		1,37	7,79
FACTORY OF FABRICS AND TEXTILE FINISHING	AMBATO	1,37	7,17
		0,76	6,04
FACTORY OF FABRICS AND TEXTILE FINISHING	AMBATO	0,71	8,66
		1,03	7,6
FACTORY OF FABRICS AND TEXTILE FINISHING	AMBATO	N-R	8,6
		1,11	7,02
FACTORY OF FABRICS AND TEXTILE FINISHING	AMBATO	1,87	6,1
FACTORY OF FABRICS AND TEXTILE FINISHING	AMBATO	N-R	8,19
		1,4	7,56
FACTORY OF FABRICS AND TEXTILE FINISHING	AMBATO	0,41	8,82
FACTORY OF FABRICS AND TEXTILE FINISHING	AMBATO	0,5	7,9
		0,3	6,74
FACTORY OF FABRICS AND TEXTILE FINISHING	AMBATO	N-R	N-R
FACTORY OF FABRICS AND TEXTILE FINISHING	AMBATO	1,64	7,56
FACTORY OF FABRICS AND TEXTILE FINISHING	AMBATO	N-R	N-R
FACTORY OF FABRICS AND TEXTILE FINISHING	AMBATO	N-R	7,55
		N-R	7,81
FACTORY OF FABRICS AND TEXTILE FINISHING	AMBATO	1,37	7,38
FACTORY OF FABRICS AND TEXTILE FINISHING	AMBATO	N-R	N-R
FACTORY OF FABRICS AND TEXTILE FINISHING	AMBATO	1,61	8,02
FACTORY OF FABRICS AND TEXTILE FINISHING	AMBATO	0,72	8,15
		0,9	7,94
		1,84	8,14
		0,59	8,22

● Maximum Flow   ● Minimum Flow   N-R: NOT REPORTED

Table A.2 Maximum reported discharging flows of factories of fabrics and textile finishing operated in
Tungurahua province.

#	Value (l/s)	#	Value (l/s)	#	Value (l/s)	#	Value (l/s)
1	3,21	17	0,84	33	0,15	49	5,61
2	1,47	18	1,72	34	0,56	50	2,75
3	2,45	19	1,68	35	2,41	51	1,72
4	0,95	20	0,73	36	1,2	52	0,75
5	3,04	21	0,12	37	3,3	53	2,04
6	2,47	22	0,98	38	1,04	54	1,37
7	2,24	23	2,03	39	1,47	55	1,03
8	0,87	24	2,16	40	1,2	56	1,11
9	4,20	25	1,8	41	0,68	57	1,87
10	2,0	26	0,79	42	2,12	58	1,4
11	0,24	27	1,9	43	0,74	59	0,41
12	1,87	28	8,88	44	1,2	60	0,5
13	3,22	29	0,44	45	2,03	61	1,64
14	1,0	30	2,43	46	2,72	62	1,37
15	3,63	31	1,9	47	1,0	63	1,61
16	1,25	32	0,81	48	5,0	64	1,84

Table A.3 Minimum reported discharging flows of factories of fabrics and textile finishing operated in
Tungurahua province.

#	Value (l/s)	#	Value (l/s)	#	Value (l/s)
1	0,15	17	0,67	33	0,76
2	0,79	18	0,72	34	0,71
3	1,21	19	0,97	35	0,3
4	0,93	20	0,17	36	0,59
5	0,81	21	0,64		
6	1,51	22	0,88		
7	0,78	23	0,14		
8	0,25	24	0,39		
9	0,77	25	1,2		
10	0,22	26	2,56		
11	1,2	27	1,96		
12	0,40	28	1,96		
13	0,14	29	1,2		
14	0,73	30	0,1		
15	0,44	31	0,12		
16	0,57	32	1,37		

Appendix B: Basis of design and Assumptions

The basis of design and the main assumptions adopted and considered in this study are described below.

- **Hydraulic Loading Rate:** The hydraulic loading rate will be five percent (5%) of the most reported effluent by the Tungurahua's textile industry. It means that the inlet flow rate of the pilot-scale filter will be 5% of the MODE of the maximum discharging flow.

- **Water retention time:** The retention time eventually must be found in a pilot plant.[86] Nevertheless, the time to allow the loading rate to pass through the filter area is 0.5 hour, and it is defined by observing the Mompiche sand kinetics regarding the photocatalytic-adsorption process reported by Gomez[13]. However, an overdesign factor (50 %) is needed to counteract any disturbance in the adsorption-photocatalytic process. Thus, the stated time is 0.75 h.

- **Filter Box:** Since the filter is targeted to be at a pilot scale, a rectangular form is considered. In this way, a ratio between the length and width of the filter must be calculated. The ratio mentioned before (a/b) for a rectangle is 1.618.[66] Thus, the ratio between the pilot-scale filter length and width must be equal to or approximately 1.618.

- **Filter medium height:** The filter modular design of this study will provide the same features of a typical sand filter. Thus, the pilot-scale and transportable sand filter will have the same sand weight percentage of a conventional sand filter. The proportionality between the sand depth and the gravel depth is 2:1.[15,17,18]

- **Head water:** The space occupied by the constant headwater will be 1.2 times the stated sand bed depth.[62,63]

- **Triangular Weir:** Level of a liquid in a vessel often is maintained by permanent or adjustable built-in weirs for the effluent. Any desired adjustment of weir height, however, can be made only on shutdown.[86] The selection of weir structures depends on the appropriate head-discharge to obtain the required performance in terms of up-stream water level. By increasing the length of the weir, the proportion of the flow passing to the weir also increases.[73] Sufficient weir length to keep the device away from flooding

and to suit changing requirements is desired. Since the filter design in this study considers the bed expansion up to 50%, the flow rate needed to expand the 50% of the sand bed is considered to calculate the flow rate to be drained during backwashing through the weir. However, an overdesign factor of 50% is considered to calculate the required capacity flow discharging of the weir.

- **Backwashing:** To backwash the sand bed with the ultimate purpose of removing deposit solids, the sand bed expansion ranges between 15% and 30%.[15] The free space forming part of the proposed freeboard in the filter is determined by stating the 50% sand bed expansion. Simply put, the filter will allow a 50% sand bed expansion before sand drainage through the triangular weir.

- **Freeboard:** The freeboard is defined as the physical space provided above the filter bed to allow its expansion during backwashing[12], and it will be approximately 15% below 500 gal and 10% above 500-gal capacity.[86] However, the freeboard it set up by the requirements of the hydraulic plant profile.[10]

- **Gravel Support:** The underdrain system requires a gravel support bed depth ranging from none to several gravel gradations. The filter bed is poured onto gravels of increasing permeability.[12] The graded gravel will have three layers: The bottom layer, the second layer, and the top layer. The gravel particle diameter varies in each layer, and the porosity and density are considered as constant. The gravel particle size in each layer is stated according to Kawamura[18] design criteria.

- **Underdrain system:** One of the fundamental purposes of the underdrain system is to collect the treated water while the granular filter media remains at rest. Perforation's diameter in the laterals are 14 mm. This fact lies in the standard hole saw drill bit is 9/16" (14 mm). Moreover, PVC is chosen to be the inert raw material for the underdrain construction. Once the filter length and width are established, the perforated laterals and their perforations must be equally spaced to warranty the flow uniformity during backwashing. Besides, the standard external diameter of the manifold and perforated laterals is 2-1/2" (6.35 cm).

Appendix C: Loss of Pressure and Head loss in Sand Filters

The head loss calculation is carried out by following the philosophy of analysis stated by Sincero[58]. First, it is important to establish that the motion of water through a filter bed is like the motion of water through parallel pipes. Figure C.1 shows a pipe of fluid and bed material. Inside this pipe, there is an element composed of fluid and bed material isolated with length dl and interstitial area A and subjected to forces as illustrated.
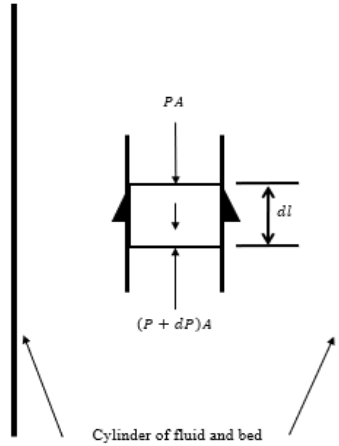
Figure C.1. Free body diagram of a pipe of fluid and bed material. Taken from Sincero[58].

The term interstitial is used because the bed is composed of grains. Thereby, the fluid is in the interstitial spaces between grains. The equation of linear momentum can be applied to the water in the downward direction of this element.

$$\sum F_z = PA - (P + dP)A + F_g - F_{sh} = \rho \boldsymbol{\varepsilon} d \forall a_z = \rho k A_s dl \frac{dv}{dt}$$

$$\sum F_z = -(dP)A + F_g + F_{sh} = \rho k A_s dl \frac{dv}{dt} \qquad (C.\ 1)$$

Where,

$$\sum F_z = Unbalanced\ force\ in\ downward\ direction\ z$$

$P = Hydrostatic\ presssure$

$A = Interstitial\ cross\ sectional\ area\ of\ the\ cylindrical\ element\ of\ the\ fluid$

$F_g = Weight\ of\ the\ fluid\ in\ the\ elemen$

$F_{sh} = Shear\ force\ acting\ on\ the\ fluid\ along\ the\ surface\ areas\ of\ the\ grains$

$\rho = Fluid\ mass\ density$

$\varepsilon = Porosity$

$d\forall = Volume\ of\ element\ of\ space$

$a_z = Aceleration\ of\ the\ fluid\ element\ in\ the\ z\ direction$

$v = Component\ fluid\ element\ velocity\ in\ the\ z\ direction$

$k = Factor\ that\ converts\ A_s\ into\ an\ area\ such\ that$

$dl = Differential\ length\ of\ the\ element$

$l = Any\ distance\ from\ some\ origin$

$A_s = Surface\ area\ of\ all\ grains$

$t = Time$

Since the fluid is in the interstitial spaces, $d\forall$ needs to be multiplied by the porosity to get the fluid volume.

The law of inertia states that a body at rest will remain at rest, and a body in uniform motion will remain in uniform motion unless acted upon by an unbalanced force. In this case, $\sum F_z = \rho k A_s dl \frac{dv}{dt}$ is considered as the unbalanced force that breaks the inertia. Hence, it is called the inertia force.

By the chain rule: $\frac{dv}{dt} = \frac{dv}{dl}\frac{dl}{dt} = v\frac{dv}{dl}$

Thus,

$$\rho k A_s dl \frac{dv}{dt} = \rho k A_s dl v \frac{dv}{dl} = \rho k A_s v dv \qquad (C.\ 2)$$

It is important to state that the velocity through the pipe could vary from the entrance to the exit. Therefore, $\bar{v}$ (constant) represents the average velocity of the varying velocity values. All the velocities took into account are interstitial velocities; it means the real velocities of the fluid as it travels through the pores.

Now, let $v^* = \frac{v}{\bar{v}}$. Hence, $dv^* = \frac{dv}{\bar{v}}$. Then,

$$\rho k A_s v dv = \rho k A_s \, (\bar{v} \, v^*) \bar{v} dv^* \qquad (C.\ 3)$$

Thus, the inertial force $\sum F_z = \rho k A_s v dv$ is proportional to $\rho k A_s \bar{v}^2$. The presence of $v^* dv^*$ does not affect this fact and it is called the proportionality constant k_i.

$$\sum F_z = k_i \rho A_s \bar{v}^2 \qquad (C.\ 4)$$

This information is considered, and the equation C.1 may now be solved for $-dPA$ ($-\Delta PA$) when applied to the whole length of the pipe.

$$-\Delta PA = k_i \rho A_s \bar{v}^2 - F_g + F_{sh} \qquad (C.\ 5)$$

Regarding F_{sh}, the Hagen-Poiseuille equation from fluid mechanics is used. This equation is written as:

$$-\Delta P_s = \frac{32 \, \mu l \bar{v}}{D^2} \qquad (C.\ 6)$$

Where,

$-\Delta P_s = Pressure\ drop\ due\ to\ shear\ forces$
$\mu = Absolute\ viscosity\ of\ the\ fluid$
$l = Length\ of\ pipe$
$D = Diameter\ of\ pipe$

It is important to mention that in a bed of grains, the cross-sectional area of flow is so small that the boundary layer created as the flow passes around one-grain overlaps with the boundary layer formed in a neighboring grain. Moreover, the boundary layer flow is, by nature, laminar, consequently flows through beds of grains is laminar, and equation C.6 can be applied.

The shear stress is $-\Delta P_s$ and thus the shear force acting on the fluid along the surface areas of the grains (F_{sh}) becomes as follows:

$$F_{sh} = -\Delta P_s A_s \qquad (C.\ 7)$$

Since the granular filter is not a pipe, so D must be replaced by the hydraulic radius r_H in equation C.6. The hydraulic radius r_H is merely defined as the area of flow divided by the wetted perimeter.

$$r_H = \frac{volume\ of\ flow}{wetted\ area} \qquad (C.\ 8)$$

Thus,

$$F_{sh} \propto \frac{\mu l \bar{v} A_s}{r_H{}^2}$$

Dimensionally, l and $r_H{}^2$ may be canceled leaving only r_H in the denominator. Then,

$$F_{sh} = k_s \frac{\mu \bar{v} A_s}{r_H} \qquad (C.9)$$

Where k_s is the overall proportionality constant.

Thus, equation C.5 becomes:

$$-\Delta PA = k_i \rho A_s \bar{v}^2 - F_g + k_s \frac{\mu \bar{v} A_s}{r_H} \qquad (C.\ 10)$$

It must be noted that for a given filter installation F_g is constant. Hence, its effect when the variables are varied is also constant. This effect will be subsumed into the values of k_i and k_s. Thereby, F_g maybe removed from the equation.

$$-\Delta PA = k_i \rho A_s \bar{v}^2 + k_s \frac{\mu \bar{v} A_s}{r_H} = A_s \left(k_i \rho \bar{v}^2 + k_s \frac{\mu \bar{v}}{r_H} \right) \qquad (C.\ 11)$$

The equation C.11 is the general linear momentum equation applied to any filter.

C.1. Head loss in grain filters

Head losses in the filter may be classified in head loss in clean filters and head loss due to the deposited materials. Since the filter designed in this project is focused on adsorption of dyes present in textile effluents, and one crucial requirement for the filter operation is the removal of total suspended solids, the head loss in clean filters is discussed.

C.2. Head loss in clean filters

To achieve the clean-filter head loss, the equation C.11 is continued by expressing A_s, r_H, and $\bar{v}$ in terms of their equivalent expressions. Let establish S_P as the surface area of a particle and N as the number of grains in bed.

Thus,

$$A_s = NS_P \qquad (C.2.\ 1)$$

Now S_o is stated as the empty bed or superficial area of the bed. Then, the volume of the bed grains (v_b) can be described as:

$$v_b = S_o\ l(1 - \varepsilon) \qquad (C.2.\ 2)$$

Let v_P represent the volume of a grain $Nv_P = v_b$. Then, N is also calculated as

$$N = \frac{S_o\ l(1 - \varepsilon)}{v_P} \qquad (C.2.\ 3)$$

Thus,

$$A_s = \frac{S_P}{v_P} S_o\ l(1 - \varepsilon) \qquad (C.2.\ 4)$$

Where,

$S_P = Surface\ area\ of\ a\ particle$

$v_P = Volume\ of\ a\ grain$

$S_o = Empty\ bed\ or\ superficial\ area\ of\ the\ bed$

$\varepsilon = Porosity$

$l = Length$

For spherical particles, $v_P = \frac{\pi d^3}{6}$ and $S_P = \pi d^2$, where d is the diameter of the particle. Therefore, $\frac{S_P}{v_P} = \frac{6}{d}$. In practice, not all particles are spherical. Thereby, the particle diameter must be converted into its equivalent spherical diameter. For other shapes or irregular particles, sphericity must be included to obtain the equivalent spherical diameter. According to McCabe et.al.[87] sphericity is defined as:

$$\Phi_s = (\frac{6}{d})(\frac{S_p}{v_p}) \qquad (C.2.\ 5)$$

In this way, according to McCabe et.al.[87] and Geankoplis[67], $\frac{S_P}{v_P}$ can be rewritten as $\frac{S_P}{v_P} = \frac{6}{\Phi_s d}$

Thus,

$$A_s = \frac{6}{\Phi_s d}\ S_o\ l(1 - \varepsilon) \qquad (C.2.\ 6)$$

The volume of the filter (v_F) can be defined as:

$$v_F = \frac{N v_P}{(1 - \varepsilon)} \qquad (C.2.\ 7)$$

Therefore, the volume of flow is: $\varepsilon * v_F = \varepsilon \frac{N v_P}{(1-\varepsilon)}$, and the wetted area may be defined as NS_P.

Then, the hydraulic radius can be described as:

$$r_H = \frac{volume\ of\ flow}{wetted\ area} = \frac{\varepsilon \frac{N v_P}{(1-\varepsilon)}}{NS_P} = \left(\frac{\varepsilon}{1-\varepsilon}\right)\left(\frac{v_P}{S_P}\right) = \left(\frac{\varepsilon}{1-\varepsilon}\right)\frac{\Phi_s d}{6} \qquad (C.2.\ 8)$$

The velocity $\bar{v}$ is the interstitial velocity of the fluid through the pores of the bed. Compared to the superficial velocity $\bar{v}_s$, $\bar{v}$ is faster due to the effect of the porosity ε. The superficial velocity is equal to the filtration rate (m/s).[11] Then, $\bar{v}$ can be defined in terms of $\bar{v}_s$ and ε as following:[58,87,88]

$$\bar{v} = \frac{\bar{v}_s}{\varepsilon} \qquad (C.2.9)$$

Substituting A_s (equation C.2.6), r_H (C.2.8), and $\bar{v}$ (equation C.2.9) in equation C.11, the following equation is obtained.

$$-\Delta PA = \frac{S_o \, l(1-\varepsilon)\bar{v}_s^2\rho}{\Phi_s d\varepsilon^2}\left(6k_i + \frac{36k_s(1-\varepsilon)}{\Phi_s d\bar{v}_s\rho/\mu}\right) \qquad (C.2.10)$$

Then,

$$-\Delta PA = \frac{S_o \, l(1-\varepsilon)\bar{v}_s^2\rho}{\Phi_s d\varepsilon^2}\left(6k_i + \frac{36k_s(1-\varepsilon)}{\Phi_s Re}\right) \qquad (C.2.11)$$

Where Re is the Reynolds number defined as: $d\bar{v}_s\rho/\mu$. According to the Ergun correlation of a mass of experimental data the terms $6k_i$ and $36k_s$ may be substituted by the values 1.75 and 150, respectively.[58,89]

Thus,

$$-\Delta PA = \frac{S_o \, l(1-\varepsilon)\bar{v}^2\rho}{\Phi_s d\varepsilon^2}\left(1.75 + \frac{150\,(1-\varepsilon)}{\Phi_s Re}\right) = \frac{S_o \, l(1-\varepsilon)\bar{v}_s^2\rho}{\Phi_s d\varepsilon^2}f_p \qquad (C.2.\,12)$$

Where f_p is a form of friction factor, and it is described as:

$$f_p = \; 1.75 + \frac{150\,(1-\varepsilon)}{\Phi_s Re} \qquad (C.2.\,13)$$

A is defined as $S_o * \varepsilon$. Then, the pressure drop across the filter is given as:

$$-\Delta P = \frac{\gamma l(1 - \varepsilon)\bar{v}_s{}^2}{\Phi_s d\varepsilon^3 g} f_p \qquad\qquad (C.2.\ 14)$$

Where,

$\gamma = Spefic\ weight\ of\ the\ fluid\ (\rho * g)$

$g = \ Gravity\ force$

The pressure drop $-\Delta P$ may be defined in terms of the equivalent height of fluid:

$$-\Delta P = \ \gamma * h_L \qquad\qquad (C.2.\ 15)$$

Where h_L represent the head loss across the filter. Thus,

$$h_L = \ \frac{l(1 - \varepsilon)\bar{v}_s{}^2}{\Phi_s d\varepsilon^3 g} f_p \qquad\qquad (C.2.\ 16)$$

Appendix D: Fluidization

Fluidization may be described as a property of particulate solids, and it represents the condition of fully suspended particles when the suspensions behave like a fluid.[87,88] When a fluid passes upward through a bed of granular solids, a pressure gradient is needed to beat the friction. If the pressure drop $(-\Delta P)$ is approximated to the weight of the bed over a unit cross-sectional area, the solids begin to move.[90] One of the foremost important advantages of using fluidization is that the fluidized solids may also be drained from the bed through pipes and valves like a liquid.[87,89]

To illustrate the fluidization phenomenon, an example proposed by McCabe et.al.[87] is provided. Consider a vertical tube partially filled with fine granular material, as shown in Figure D.1 The tube is open at the top and presents a porous plate at the bottom to support the bed of granular material. The porous plate also distributes the flow uniformly over the entire cross-section. If air is admitted below the distributor plate at a low rate of flow, it passes upward through the bed causing any particle motion. If the solid particles are small enough, flow in the channels between the particles will be laminar, and the drop of pressure across the granular bed will be proportional to the superficial velocity V_O. If the flow velocity is gradually increased, the pressure drop increases and the height remains constant because the particles are still fixed. At a particular velocity, the pressure drop across the bed becomes equal to the force of gravity on the particles. At this time, minimum fluidization velocity is achieved, and any longer increase in the fluid velocity induce particle motion. Also, when fluidization begins, the porosity of the bed is the minimum porosity for incipient fluidization. In other words, the bed expands a little to achieve the minimum void fraction before particle motion occurs. The minimum porosity may be determined experimentally. Sometimes the bed expands with the grains still in contact, since a small increase in porosity may compensate for a rise in fluid velocity and keep the loss of pressure constant. With an additional increase in flow velocity, the particles become separated to move about in the bed, and true fluidization begins.[67,87]
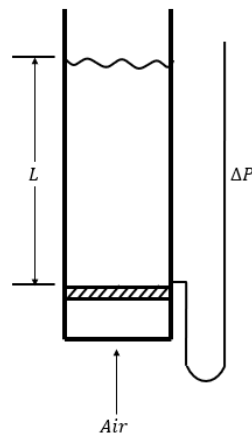
Figure D.1. Vertical tube partially filled with fine granular material. Taken from McCabe et.al.[87]

In the fluidized bed, the pressure drop across the bed remains constant, but the bed height continues to increase with the increasing flow velocity. At this point, if the flow velocity is gradually reduced, the pressure drop stays constant, and the bed height decreases. Nevertheless, the final bed height may be higher than the initial height of the fixed bed. This fact lies in solids dumped in a tube tend to pack more tightly than solids slowly settling from a fluidized state.[87]

D.1 Minimum Fluidization Velocity

The equation to calculate the minimum fluidization velocity may be obtained by settling the pressure drop across the bed is equal to the weight of the bed per unit area of cross-section

$$\Delta P = g\,(1 - \varepsilon)\big(\rho_p - \rho\big)l \qquad\qquad (D.1.\ 1)$$

Where,

ρ_p = The density of the particles.

ρ = Density of the fluid.

ε = Void Fraction

g = Gravity

l = Length used by the whole bed of particles.

At initial fluidization, ε is the minimum porosity ε_M.

Thus,

$$\frac{\Delta P}{l} = g\ (1 - \varepsilon_M)\big(\rho_p - \rho\big) \qquad\qquad (D.1.\ 2)$$

The equation D.1.2 can be rewritten as:

$$\frac{\Delta P}{l} = \frac{(1 - \varepsilon)\rho\bar{v}_s{}^2}{\Phi_s d\varepsilon^3}\left(1.75 + \frac{150\ \mu(1 - \varepsilon)}{\Phi_s d\bar{v}_s\rho}\right) \qquad\qquad (D.1.\ 3)$$

Applying the equation D.1.2 and D.1.3 to the point of initial fluidization, a quadratic equation for the minimum fluidization velocity V_{oM} is obtained.

$$g\ (1 - \varepsilon_M)\big(\rho_p - \rho\big) = \frac{(1 - \varepsilon_M)\rho\bar{v}_{oM}{}^2}{\Phi_s d\varepsilon_M{}^3}\left(1.75 + \frac{150\ \mu\ (1 - \varepsilon_M)}{\Phi_s d\bar{v}_{oM}\rho}\right) \qquad (D.1.\ 4)$$

Then,

$$g\ (\rho_p - \rho) = \left(1.75\frac{\rho\bar{v}_{oM}{}^2}{\Phi_s d\varepsilon_M{}^3} + \frac{150\ \mu\bar{v}_{oM}(1 - \varepsilon_M)}{\Phi_s{}^2 d^2\varepsilon_M{}^3}\right) \qquad\qquad (D.1.\ 5)$$

As equation D.1.5 comes from the Ergun equation, only the laminar-flow term, given by the Kozeny equation, is significant for small particles.[67,87] In other words, if the fluid is laminar, the first term of the equation dominates. Otherwise, the second term of the equation dominates if the fluid is tortuous.[89]

Thus,

$$\bar{v}_{oM} = \frac{g\big(\rho_p - \rho\big)\Phi_s{}^2 d^2\varepsilon_M{}^3}{150\ \mu\ (1 - \varepsilon_M)} \qquad\qquad (D.1.\ 6)$$

When a fluid passes through a bed of particles, three effects are caused as a function of fluid velocity. These effects are observed as at low fluid velocities the bed may expand a little, but the particles still remain stationary, higher velocities cause the particles to become supported

in the fluid, and the particles also become suspended in the liquid and can be transported within it.[88]

The equation D.1.6 to obtain the minimum fluidization velocity is applied to liquids and gases. However, if the $\bar{v}_{oM}$ increases, the fluidization by liquid and gases causes different behaviors in the fluidized beds. Hence, the fluidization may be divided into particulate and bubble fluidization. In general, particulate fluidization is observed in solid-liquid systems and solid-gas systems when the particles are very small and only over a limited range of fluid velocities. If sand is fluidized with water, particulate fluidization occurs. If the fluid velocity increases above the minimum fluidization velocity, the bed of particles will continue to expand, and the porosity of the bed will increase.[87,88,90]

D.2. Expansion of fluidized beds

As stated before, the bed continues to expand with increasing velocities. If the fluid velocity is increased when the fluidization point has been achieved, the pressure drop remains constant, and the bed porosity increases.[67,87] At this point, the transport of the solids may occur with adequate fluid velocity.[88] The expansion of the fluidized beds is uniform in particulate fluidization. Considering the flow between the particles as laminar, the following equation may be applied for expanded beds.[87]

$$\frac{\varepsilon^3}{1-\varepsilon} = \frac{150\,\mu\bar{v}_o}{g(\rho_p - \rho)\Phi_s^{\,2}d^2} \qquad (D.2.\,1)$$

The equation D.2.1 is analogous to the equation used for the minimum fluidization velocity, but now $\bar{v}_o$ is the independent variable. Thereby, notice that $\frac{\varepsilon^3}{1-\varepsilon}$ is proportional to $\bar{v}_o$ for values above $\bar{v}_{oM}$.[87]

Then, the relation between bed height and porosity can be obtained. The volume $LA(1-\varepsilon)$ is equal to the total volume of solids considered as one piece.[67]

Thus,

97

$$L_1 A(1 - \varepsilon_1) = L_2 A(1 - \varepsilon_2) \qquad\qquad (D.2.\ 2)$$

Where:

$L_1 = $ Is the height of the bed with porosity ε_1
$L_2 = $ Is the height of the bed with porosity ε_2
$A = $ Entire cross-sectional area occupied by the solid particles

Then,

$$\frac{L_1}{L_2} = \frac{1 - \varepsilon_2}{1 - \varepsilon_1} \qquad\qquad (D.2.\ 3)$$

At incipient fluidization,

$$L = L_M \frac{1 - \varepsilon_M}{1 - \varepsilon} \qquad\qquad (D.2.\ 4)$$

Then, the height of the expanded bed with a particular porosity can be calculated.

Appendix E: Triangular Weir

A side weir may be defined as a structure which allows part of a fluid to be spilled over the side. Side weirs may be constructed in different shapes like rectangular, triangular, trapezoidal, etc. and they are commonly used in sewage systems, irrigation, land drainage, and storm relief.[91] Thin plate weirs allow an accurate discharge measurement with straightforward instruments. The V-notch weir is also named triangular weirs, and they present an overflow edge in the form of an isosceles triangle.[92]

Typically, the channel upstream from the weir has to be straight, smooth, horizontal, and rectangular with enough length to develop a uniform flow and velocity distribution for all discharges.[93]

The traditional equation for flow discharging in V-notch weirs is derived based on an assumed analogy between the weir and the orifice, it is dimensionally correct and is expressed as:[94]

$$Q = C * \frac{8}{15} * \tan\frac{\phi}{2} * \sqrt{2 * g * h^5} \qquad (E.\ 1)$$

Where,

Q = Flow rate of water discharge
C = A dimensionless discharge coefficient
ϕ = The notch opening angle
g = Gravity acceleration
h = Upstream water height above the notch

It has been shown that C is a function of all variables needed to describe the channel, the weir, and the liquid. In the absence of a theoretical solution, dimensional relations must be applied to analyze the experimental data.[92,94] However, some studies have been developed to determine the discharge coefficients in weirs for different liquids.

The main variables needed to state the discharge characteristics of a triangular notch are described below.[94]

$$Q = f(B, P, h, \phi, \rho, \mu, \sigma, \gamma) \qquad (E.\ 2)$$

Where,

Q = Discharge

B = With of the approach channel

P = Height of the notch vertex concerning the floor of the channel

h = The head on the weir referred to the vertex of the notch

ϕ = Opening notch angle

ρ = Density of the liquid

μ = Viscosity of the liquid

σ = Surface tension of the liquid

γ = Specific weight of the liquid

Starting from the equation E.1 , a non-dimensional discharge ratio may be expressed as:[94]

$$\frac{Q}{h^2 \sqrt{h(\frac{\gamma}{\rho})}} = f(\frac{h}{P}, \frac{h}{B}, \phi, R, W) \qquad (E.\ 3)$$

The dependent ratio in equation E.3 is proportional to the coefficient of discharge. On the right hand of the equation, the first three ratios describe the geometry of the weir, approach channel, and flow pattern. The other two ratios are the Reynolds number (R) and the Weber number (W). Over a limited range of temperature, μ, ρ, and σ may be assumed as constant values for one liquid. Thereby, R and W in equation E.3 may be replaced by h.[94]

Thus,

$$C = f(\frac{h}{P}, \frac{P}{B}, \phi, h) \qquad (E.\ 4)$$

However, some studies have been developed to determine the discharge coefficients in weirs for different liquids.

Furthermore, John Shen[94] proposed an adjustment of measured values of h. Thus, the equation E.1 may be rewritten:

$$Q = C * \frac{8}{15} * \tan\frac{\phi}{2} * \sqrt{2 * g * h_e^{5}}$$

<div align="right">(E. 5)</div>

Where h_e is called the effective head and it is determined by the equation:

$$h_e = h + k$$

<div align="right">(E. 6)</div>

To calculate the k value, the following equation is considered:

$$k = \frac{0.002}{\sin(\frac{\phi}{2})}$$

<div align="right">(E. 7)</div>

It is essential to state that the use of h instead of h_e is considerable only for small values of h. [94] Experiments carried out by Professor Arno T. Lenz at the University of Wisconsin, derived the equation E.5 to determine C for water at (70°F) in which n and a are a function of ϕ alone. The values of n and a were determined experimentally and are shown in Table E.1.[94]

$$C = 0{,}560 + \frac{n}{h^a}$$

<div align="right">(E. 2)</div>

Table E.1 Values of n and a for equation E.5.[94]

Constant	Notch Angle, ∢					
	90°	60°	45°	28°04'	20°	10°
n	0.0159	0.0203	0.0238	0.0315	0.0390	0.0624
a	0.588	0.582	0.579	0.575	0.573	0.569

Since the water level in the parent channel does not remain stationary, it may rise or fall along the length of the weir according to the flow conditions.[73] The weir notch is placed just above the freeboard to drain backwashed. Moreover, sufficient space is available below the triangular weir to allow the fluidization of the sand bed and zeolite. In this way, sand bed and zeolite may be drained by fluidization if needed. If the filter bed gets clogged and the inlet water raises its level inside the tank, weir will be a sewage system and avoid flooding.

Appendix F: Filter Pressure

F.1 Horizontal Pressure

While designing storage tanks, ships, dams, and other hydraulic structures, the forces developed on a surface due to the fluid must be known. At rest-condition, the pressure varies linearly with depth if the fluid is incompressible. For the horizontal surface of the bottom of a liquid-filled tank (Figure F.1.1), the magnitude of the resultant force is described by the equation F.1.1.
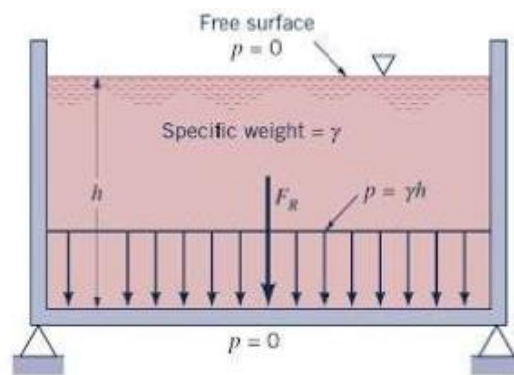

Figure F.1.1. Force exerted by water on the bottom of a tank. Taken from Gerhart [95].

$$F_R = P * A = \gamma * h * A$$
<div align="right">*(F.1. 1)*</div>

Where,

F_R = Resultant Force
P= Uniform Pressure on the bottom
A= Area of the bottom
γ= Specific Weight of the fluid
h= Depth form the surface to the bottom

Regarding the horizontal pressure exerted by the solid medium, the vertical stress is equal to the weight of the solid lying directly at the point where the solid is at rest. Considering the unit weight of the solid (γ_s) as constant with depth, the vertical stress can be defined as:[96]

$$\sigma_v = \gamma_s * h \qquad\qquad\qquad (F.1.\,2)$$

Where,

γ_s= Specific Weight of the solid

h= Depth form the surface to the bottom

F.2 Pressure on Vertical Surfaces

Figure F.2.1 shows the pressure distribution along the vertical face of a tank with constant width, which contains a liquid having a specific weight γ. Since the pressure varies linearly with depth, it is equal to zero at the top and equal to $\gamma * h$ at the bottom. [95]
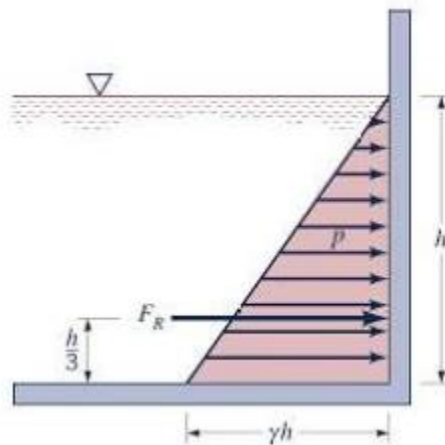

Figure F.2.1. Force exerted by water on the vertical face of a tank. Taken from Gerhart[95].

The average pressure is exerted at $h/2$. Thus, the resultant force acting on a rectangular area (A) is described as following:[95,97]

$$F_R = P_{av} * A = \gamma * \left(\frac{h}{2}\right) * A \qquad\qquad (F.2.\,1)$$

Where,

P_{av}= The average pressure

A= Rectangular Area

h= Depth from the top

103

γ= Specific Weight

Regarding the pressure exerted in the vertical walls by the filter medium, basic equations of soil mechanics are stated. Commonly, lateral forces develop against structures supporting or containing soil or water. When designing these kinds of structures, the pressure of both soil and water must be considered.[96] The lateral pressure against the walls depends on the movement of the walls relative to the soil mass. If the wall does not move, the at-rest condition is considered. The lateral earth pressure σ_H can be expressed as:[96,98,99]

$$\sigma_H = K\sigma_v \qquad\qquad\text{(F.2. 2)}$$

Where,

σ_H= Horizontal Pressure
K= Coefficient of Lateral Earth Pressure
σ_v= Vertical Pressure

For the at-rest the condition,

$$K = K_0 \qquad\qquad\text{(F.2. 3)}$$

Where, K_0= Coefficient of lateral stress at rest

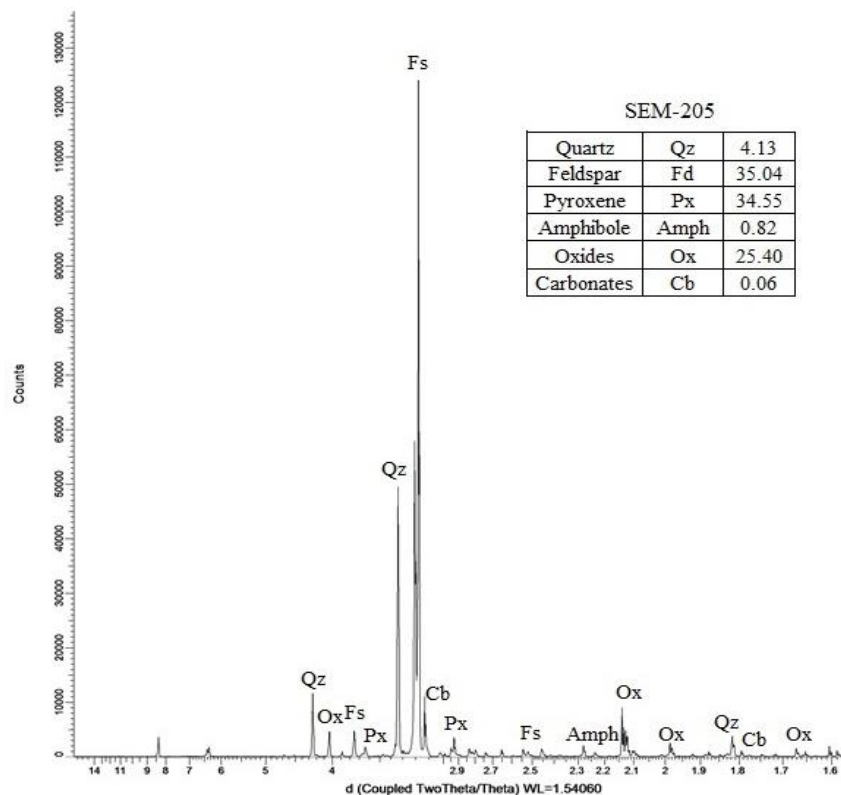# Appendix G: Characterization of Mompiche black sand (SEM-205) of Ecuador

Figure G.1. X-Ray Diffraction Pattern for Mompiche natural sand (SEM-205). The inset includes the percentage of mineral phase in the sample. Taken from Vera[54].

Table G.1. Particle Size information of Iron-titaniferous ecuadorian sands where Mompiche sand (SEM-205) is included.[54]

Sample	Surface area (cm2/cm3)	Median size (um)	Mean size (um)	Transmittance /R (%)	Transmittance /B (%)
SXQ-101	793.49	134.11	142.74	82.4	81.7
SXQ-102	2623.7	95.12	98.98	84	85.1
SYA-103	163.54	383.07	548.90	86.5	89.4
SYA-104	179.36	349.74	558.64	85.1	88.4
SYO-105	308.89	176.57	756.65	80.5	85.8
SYM-106	218.19	257.12	747.28	88.9	91.7
SEV-201	1961.5	298.46	1364.26	81.5	76.7
SET-202	255.6	277.40	582.91	86.6	89.3
SET-203	278.89	219.45	479.99	87.3	89.6
SMP-204	311.08	173.10	939.61	84.8	84.6
SEM-205	336.57	172.03	548.78	82.8	84.2